Physics – Uspekhi **44** (3) 255 – 284 (2001)

REVIEWS OF TOPICAL PROBLEMS PACS numbers: **61.30. – v**, 83.70.Jr, 83.85.Jn

Physical methods for measuring the viscosity coefficients of nematic liquid crystals

V V Belyaev

DOI: 10.1070/PU2001v044n03ABEH000831

Contents

Abstract. Methods for measuring the viscosity coefficients of the best known type of anisotropic fluid, nematic liquid crystals (NLCs), are reviewed. The hydrodynamic Leslie – Ericksen – Parodi theory is described in brief, which predicts five independent viscosity coefficients for a NLC. The feature that distinguishes NLCs from isotropic liquids is the rotational viscosity, due to energy dissipation caused by NLC reorientation. The shear flow method, methods based on ultrasonic wave propagation and absorption in an anisotropic medium, and the rotating magnetic field technique are described in detail, as well as methods that involve analyzing the Freedericksz transition dynamics (LC reorientation in an electric or magnetic field) and those using light scattering from the thermal fluctuations of the NLC director. In each case, the accuracy of the method is evaluated, its complexity assessed, and the amount of material needed for measurement estimated.

1. Introduction

Liquid crystals (also called mesogens or anisotropic fluids) are materials retaining a long-range orientational order of their molecules. Nematic liquid crystals (NLCs) are mesogens lacking a long-range translational order. Other liquid-crystal phases have either a lamellar (smectics) or twisted (cholesterics) structure.

V V Belyaev Central R&D 'Cometa'
ul. Velozavodskaya 5, 109280 Moscow, Russian Federation
Tel. (7-095) 274-09 61
Fax (7-095) 274-08 70
E-mail: vbelyaev@mtu-net.ru

Received 17 July 2000, revised 16 November 2000
Uspekhi Fizicheskikh Nauk **171** (3) 267 – 298 (2001)
Translated by Yu V Morozov; edited by A V Getling

The liquid-crystalline state of matter attracts the attention of researchers and engineers for two reasons. One is related to its practical implications due to the high optic sensitivity of liquid crystals (LCs) to electric field variations at an extremely low driving voltage and their low power consumption. The light undergoes complete modulation even when the voltage applied to an LC layer varies from a few hundredths to a few tenths of a volt. The other reason pertains to an unusually high diversity of physical effects of LCs dictated by their structure. Electrooptical effects of LCs have been described by L M Blinov and V G Chigrinov [1], their structure and physical effects by S Chandrasekhar [2], and physicochemical properties in the books by W H de Jeu [3] and M F Grebenkin and A V Ivashchenko [4]. The last two monographs consider a number of NLC properties including viscosity, the subject matter of the present review. The interest in viscosity is attributable to the practical importance of this property, which is employed in fast-acting liquid-crystal devices, and to the scientific results brought about by the study of LC flows and reorientation. Unlike [3, 4], the present review is focused on various methods for the measurement of the LC viscosity coefficients. It describes state-of-the-art approaches to the problem. At the same time, I could not resist the temptation of describing the classic experiments of Miesowicz and Tsvetkov first reported in the 1930s and retaining their value till now. Also reviewed are numerous studies performed in the Soviet Union, CIS, and other countries. Many of them have been published in editions that are not readily available at present.

The author sought to make the review both complete and rigorous, so that it would serve not only for reference but also for posing and solving problems related to the viscosity of nematic and other liquid-crystal phases and to the liquid state at large. A consideration of the relationships between viscosity, thermodynamic parameters (temperature, pressure) and molecular structure is beyond the scope of this review.

2. Anisotropy of viscosity coefficients of liquid crystals

The orientation of nematic liquid crystals is characterized by a unit vector **n** parallel to the distinguished direction determined by the orderly aligned long axes of NLC molecules. This vector is called the director. The degree of LC regularity (or the order parameter) depends on the deviation of the orientation of the long axes from that of the director:

$$S = \frac{3\langle\cos^2\theta\rangle - 1}{2}\,, \tag{2.1}$$

where θ is the angle formed by the long axis of a molecule and the director. In the crystalline phase, $S = 1$; in the isotropic one, $S = 0$; and in the liquid-crystalline state, $(0.3 \text{ to } 0.4) < S < 1$.

The existence of a distinguished direction along which LC molecules are aligned accounts for the anisotropy of virtually all LC properties, including viscosity. It is also responsible for the appearance of viscosity coefficients that have no analogues in isotropic fluids.

The hydrodynamic theory of NLCs has been consistently developed by Ericksen [5], Leslie [6], and Parodi [7]. For an incompressible, thermally insulated medium kept at a constant temperature, the equations of motion include four conservation laws governing mass, energy, momentum, and angular momentum. Let the fluid enclosed in a volume V bounded by the surface A have the density ρ. The major difference of the equations for nematics, given below, from the corresponding equations for isotropic fluids consists in the fact that they include orientational movement of the director **n**, except the progressive motion of the fluid with a velocity v_i (i, j, k are the spatial coordinates). For this reason, the equations of nematodynamics include such variables as the velocity (v_i) and director (n_i) fields as well as their gradients $v_{i,j}$ and $n_{i,j}$ and time derivatives $\dot{v}_i$ and $\dot{n}_i$. Equations for the conservation of mass and momentum (continuity) can be written as follows [2, 6]:

$$\frac{\mathrm{d}}{\mathrm{d}t}\int_V \rho\,\mathrm{d}V = 0\,, \tag{2.2}$$

$$\frac{\mathrm{d}}{\mathrm{d}t}\int_V \rho v_i\,\mathrm{d}V = \int_V f_i\,\mathrm{d}V + \int_A \sigma_{ji}\,\mathrm{d}A_j\,, \tag{2.3}$$

where f_i is the force acting on unit volume and σ_{ij} is the stress tensor. In the energy- conservation law

$$\frac{\mathrm{d}}{\mathrm{d}t}\int_V \left(\frac{1}{2}\rho v_i\, v_i + U + \frac{1}{2}\rho_I \dot{n}_i\,\dot{n}_i\right)\mathrm{d}V = \int_V (f_i\, v_i + G_i\,\dot{n}_i)\,\mathrm{d}V + \int_A (\sigma_i\, v_i + s_i\,\dot{n}_i)\,\mathrm{d}A\,, \tag{2.4}$$

ρ_I is the moment of inertia per unit volume, U is the internal energy, G_i is the external torque density acting on the director, $\sigma_i = \sigma_{ij} v_j$ is the surface force per unit area (v_j is the normal to the plane), and $s_i = \pi_{ij} v_j$ is the torque per unit area. Taking into account the equation of angular-momentum conservation

$$\frac{\mathrm{d}}{\mathrm{d}t}\int_V (\rho\, e_{ijk}\, x_j v_k + \rho_I\, e_{ijk}\,\dot{n}_j\,\dot{n}_k)\,\mathrm{d}V = \int_V (e_{ijk}\, x_j f_k + e_{ijk}\,\dot{n}_j G_k)\,\mathrm{d}V + \int_A (e_{ijk}\, x_j \sigma_k + e_{ijk}\, n_j\, s_k)\,\mathrm{d}A \tag{2.5}$$

makes it possible to derive the Oseen equation

$$\int_V \rho_I\,\ddot{n}_i\,\mathrm{d}V = \int_V (G_i + g_i)\,\mathrm{d}V + \int_A \pi_{ij}\,\mathrm{d}A_j\,, \tag{2.6}$$

where the right-hand side represents the final effect of all external (G_i) and internal (g_i) volume and surface (π_i) forces acting on the director. The transformation and simplification of integrals (2.2)–(2.6) give the following system of differential equations:

$$\begin{aligned}
&\dot{\rho} = 0\,,\\
&\rho\dot{v}_i = f_i + \sigma_{ji,j}\,,\\
&\dot{U} = \sigma_{ji} A_{ij} + \pi_{ji} N_{ij} - g_i N_i\,,\\
&\rho\ddot{n}_i = G_i + g_i + \pi_{ij,i}\,,
\end{aligned} \tag{2.7}$$

where

$$\sigma_{ji} - \pi_{kj}\, n_{i,k} + g_j\, n_i = \sigma_{ij} - \pi_{ki}\, n_{j,k} + g_i\, n_j\,, \tag{2.8}$$

$$N_i = \dot{n}_i - \Omega_{ik} n_k \;\; (\text{in the vector form } \mathbf{N} = \dot{\mathbf{n}} - \boldsymbol{\omega}\times\mathbf{n} = (\boldsymbol{\Omega} - \boldsymbol{\omega})\times\mathbf{n},\;\; \boldsymbol{\omega} = \frac{1}{2}\operatorname{rot}\mathbf{v})\,, \tag{2.9}$$

$$N_{ij} = \dot{n}_{i,j} - \Omega_{ik}\, n_{k,j}\,, \tag{2.10}$$

$$A_{ij} = \frac{1}{2}\left(\frac{\partial v_j}{\partial x_i} + \frac{\partial v_i}{\partial x_j}\right), \tag{2.11}$$

$$\Omega_{ij} = \frac{1}{2}\left(\frac{\partial v_j}{\partial x_i} - \frac{\partial v_i}{\partial x_j}\right). \tag{2.12}$$

The vector **N** represents the angular velocity of the director relative to the fluid.

The terms of the system of equations (2.2)–(2.6) or (2.7) that describe the orientational movement of the director are of the same order of magnitude as and frequently larger than the corresponding terms for the translatory fluid motion. In other words, they can be interpreted as flows or forces [2]. It will be shown below that their contribution strongly depends on the director orientation with respect to real streams.

Information about NLC viscosities is contained in the antisymmetric viscous-stress tensor σ_{ij} and vector g_i that corresponds to the internal volume force acting on the director. As the first step towards the determination of their form, the following inequality for the free energy can be obtained based on the increase in the system entropy:

$$\sigma_{ji} A_{ij} + \pi_{ji}\, N_{ij} - g_i N_i - \dot{F} \geqslant 0\,. \tag{2.13}$$

Thereafter, the free energy can be expanded in powers of the director n_i, its gradients $n_{i,j}$, angular velocity N_i, and velocity gradient (or the symmetric tensor A_{ij}, to be more precise). Distinguished in tensor σ_{ij} and vector g_i are components corresponding to isothermal static deformation —

$$\sigma^0_{ji} = -p\delta_{ji} - \frac{\partial F}{\partial n_{k,i}}\, n_{k,i}\,\delta_{ij}\,, \qquad g^0_i = \mu n_i - \beta_j\, n_{i,j} - \frac{\partial F}{\partial n_i}\,,$$

(where p and μ are arbitrary constants) — and those corresponding to the hydrodynamic part of the deformation (σ'_{ji} and g'_i). The hydrodynamic components σ'_{ji} and g'_i can be

expanded in powers of n_i, N_i, and A_{ij}:

$$\sigma'_{ij} = K^0_{ji} + K^1_{jik} N_k + K^2_{jikm} A_{km} ,$$
$$g'_i = L^0_i + L^1_{ij} N_j + L^2_{ijk} A_{jk} , \quad (2.14)$$

where K and L are the director functions. The coefficients of expansion of these functions in n_i have the dimension of viscosity. A series of transformations of (2.14) taking into consideration physical reasons leads to the final expression for the hydrodynamic component of the viscous stress tensor with the Leslie viscosity coefficients α_i $(i = 1-6)$:

$$\sigma'_{ji} = \alpha_1 n_k n_m A_{km} n_i n_j + \alpha_2 n_j N_i + \alpha_3 n_i N_j + \alpha_4 A_{ji} + \alpha_5 n_j n_k A_{ki} + \alpha_6 n_i n_k A_{kj} \quad (2.15)$$

and for the corresponding vector of the internal volume force:

$$g'_i \equiv \gamma_1 N_i + \gamma_2 n_j A_{ji} , \quad \gamma_1 = \alpha_3 - \alpha_2 , \quad \gamma_2 = \alpha_5 - \alpha_6 . \quad (2.16)$$

The prototype expressions originally obtained by Leslie in 1966 [6] are as follows:

$$\sigma' = \alpha_1 (\mathbf{n}\cdot\mathbf{n}:\bar{\bar{A}})\mathbf{n}\cdot\mathbf{n} + \alpha_2 \mathbf{n}\cdot\mathbf{N} + \alpha_3 \mathbf{N}\cdot\mathbf{n} + \alpha_4 \bar{\bar{A}} + \alpha_5 \mathbf{nn}.\bar{\bar{A}} + \alpha_6 \bar{\bar{A}}.\mathbf{nn} , \quad (2.17)$$

$$g' = \gamma_1 \mathbf{N} + \gamma_2 \bar{\bar{A}}.\mathbf{n} . \quad (2.18)$$

The following notation was used in [6]: (ab) has components $(ab)_{\alpha\beta} = a_\alpha b_\beta$, $ab:A = a.A.b = a_\beta b_\beta A_{\alpha\beta}$, $(A.ab)_{\alpha\beta} = A_{\alpha\gamma} a_\gamma b_\beta$.

In view of the Parodi relation (see [7]) derived from the expression for the entropy growth (dissipation) rate and the Onsager reciprocal relations for irreversible processes,

$$\alpha_2 + \alpha_3 = \alpha_6 - \alpha_5 , \quad (2.19)$$

five NLC viscosity coefficients are independent.

Let us scrutinize expressions (2.17), (2.18). It follows from the expression for σ'_{ji} that the fourth term in the right-hand side is only determined by the fluid velocity field and contains no information about the director. Coefficient α_4, the analogue of the isotropic viscosity coefficient, is always positive. Terms with the director angular velocity N_j contain viscosity coefficients α_2 and α_3. For nematics formed by elongated rod-like molecules, these coefficients are negative, in correspondence with increases (rather than decreases) in the deformation of the director in a fluid flow (see below for more detail). Both coefficients, α_2 and α_3, appear in the terms that contain neither velocities nor their gradients; that is, they are related only to the director reorientation. This primarily refers to their combination $\gamma_1 = \alpha_3 - \alpha_2$, also known as the coefficient of NLC rotational viscosity or Tsvetkov's viscosity coefficient. It will be shown below that the rotational viscosity describes the director rotation in the absence of any flow. In an NLC, coefficients α_5 and α_6 have opposite signs, with $\alpha_5 > 0$ and $\alpha_6 < 0$. The coefficient α_1 corresponds to tensile strain. It is negative for nematics composed of elongated rod-like molecules. Moreover, the following relations between the Leslie coefficients follow from (2.13)-type inequalities associated with entropy growth:

$$2\alpha_1 + 3\alpha_4 + 2\alpha_5 + 2\alpha_6 \geqslant 0 ,$$
$$2\alpha_4 + \alpha_5 + \alpha_6 \geqslant 0 ,$$
$$4\gamma_1(2\alpha_4 + \alpha_5 + \alpha_6) \geqslant (\alpha_2 + \alpha_3 - \gamma_2)^2 . \quad (2.20)$$

Ref. [8] describes the overall hydrodynamic pattern of systems with a long- or short-range spatial order (crystals, smectics, nematics, ordinary liquids, and glasses) responsible for an increase in the number of coefficients characterizing transport phenomena (thermal conduction and viscosity). Table 1, borrowed from this work, shows the number of variables that appear in the hydrodynamic theories of various systems.

It is worthwhile to mention that a paper by Forster [9] contains an alternative description of NLC hydrodynamics, which takes into account acoustic wave propagation. According to [8–10], a nematic LC is characterized by the tensor field of the orientational order parameter

$$Q_{ij} = Q\left(n_i n_j - \frac{1}{3}\,\delta_{ij}\right) .$$

The principal axis of tensor Q_{ij} is the molecular orientational axis, while $Q = S$. However, the spectrum of fluctuations in the variables considered by the hydrodynamic theory contains only low frequencies, which occur only in the director fluctuation spectrum rather than in the spectrum of order parameter fluctuations. In the Forster theory, the viscous stress tensor has the form

$$\sigma^1_{ij} = 2\nu_2 A_{ij} + 2(\nu_3 - \nu_2)(A_{ik} n_k n_j + A_{jk} n_i n_k) + (\nu_4 - \nu_2)\delta_{ij} A_{kk} + (\nu_1 + \nu_2 - 2\nu_3) n_i n_j n_k n_l A_{kl} + (\nu_5 - \nu_4 + \nu_2)(\delta_{ij} n_k n_l A_{kl} + n_i n_j A_{kk}) . \quad (2.21)$$

Table 1. Number of selected thermodynamic parameters in different monoatomic (monomolecular) systems.

Phase	Number of independent hydrodynamic variables	Number of viscosity coefficients η_{ijkl}		Transport coefficients		Dissipation coefficients (for NLC $\zeta \sim \gamma_1^{-1}$)	Number of parameters describing relationships between the order parameter and flow
		total	in an incompressible system	thermal conductivity $\varkappa_{ij}$	ξ_i^α		
Simple liquid	5	2	1	1	0	0	0
Nematic	7	5	3	2	0	1	1
Smectic *A* and cholesteric	6	5	3	2	1	1	0
Smectic *B* (uniaxial)	8	5	3	2	2	2	0
Uniaxial crystalline	8	5	3	2	2	2	0
Smectic *C*	7	13	9	4	2	2	2
General crystalline	8	21	15	6	9	6	0
Cubic crystalline	8	3	2	1	1	1	0
Glass	8	2	1	1	1	1	0

Unlike the situation with the Ericksen – Leslie – Parodi approach, the quantities $A_{\alpha\beta}$ and n_α in (2.21) appear as forces and the quantities $\sigma_{\alpha\beta}$ and N_α as flows. In this expression, v_1, v_2, v_3 are coefficients of shear viscosity and $v_4 - v_2$, v_5 are the coefficients of volume viscosity. For an incompressible medium, $v_4 = v_2$, $v_5 = 0$.

The Ericksen – Leslie – Parodi theory is discussed at greater length in the book by Chandrasekhar [2] and the theory of Forster and his co-workers, in volume 7 of 'Theoretical Physics' by Landau and Lifshitz [11]. In Ref. [12], a system of equations is given which takes into account volume deformations along with shear and orientation deformations of LCs under external pressure. We note that the requirements for the orientational distribution function posed by the Ericksen – Leslie – Parodi approach are examined in [13]: it must be uniaxial and have the form of a δ function. Equations of the orientational equilibrium for two-dimensional LCs and LCs composed of biaxial molecules are presented in [14, 15].

3. Relationship between LC shear flow and director rotation

It is not the Leslie coefficients α_i which are determined experimentally, but the coefficients of viscosity for an NLC flow with a constant velocity gradient (or constant shear rate) and the coefficient of viscosity describing director rotation.

Let a liquid crystal flow between two parallel plates and the director orientation be specified by an external (e.g. magnetic) field. Then, as shown in [3,16], the viscosity is described by the following expression:

$$\eta(\theta,\varphi) = (\eta_1 + \eta_{12}\cos^2\theta)\sin^2\theta\cos^2\varphi + \eta_2\cos^2\theta + \eta_3\sin^2\theta\sin^2\varphi\,, \tag{3.1}$$

where θ is the angle between the stream direction and the director and φ is the angle between the velocity gradient and the projection of the director onto the plane formed by the vectors $\nabla\mathbf{v}$ and $\mathbf{n}\times\nabla\mathbf{v}$ ($\mathbf{v}$ is the flow velocity). It is possible to measure four NLC viscosity coefficients for four different flow geometries (Fig. 1): η_1 when the director is parallel to the velocity gradient; η_2 when the director is parallel to the stream velocity direction; η_3 when the director is normal to the shear plane, i.e. the plane in which the vectors of velocity gradient $\nabla\mathbf{v}$ and velocity $\mathbf{v}$ lie; and $\eta_{45^\circ} = 0.5(\eta_1+\eta_2) + 0.25\eta_{12}$ when the director is in the shear plane and forms an angle of 45° with the vectors $\mathbf{v}$ and $\nabla\mathbf{v}$ (in this case, the contribution of the tensile strain is maximum).

The anisotropy of viscosity coefficients in a shear flow was first reported by Miesowicz [17]. Therefore, coefficients η_i ($i = 1, 2, 3$) are frequently referred to as Miesowicz coefficients of viscosity. The relationship between these coefficients and the Leslie coefficients of viscosity can be established by substituting the director components and velocity gradients into (2.15) and is described by the expressions

$$\eta_1 = 0.5(\alpha_4+\alpha_5-\alpha_2)\,,\quad \eta_2 = 0.5(\alpha_3+\alpha_4+\alpha_6)\,,$$
$$\eta_3 = \alpha_4\,,\quad \eta_{12} = \alpha_1\,. \tag{3.2}$$

All the Miesowicz coefficients except η_{12} are positive.

The solution of a similar problem for another LC flow type demonstrates that the stream determines the director orientation. In the case of a stationary, laminar (Poiseuille) NLC flow in a cylindrical pipe, induced by a pressure gradient

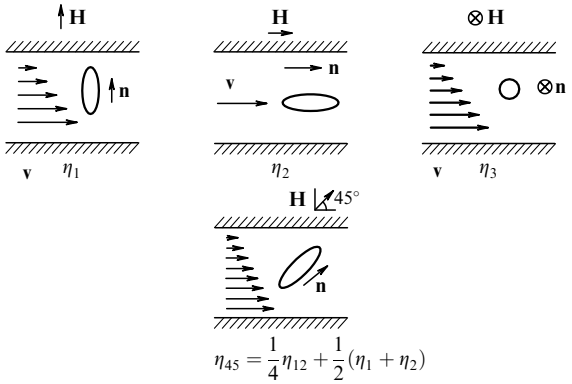

Figure 1. Relative disposition of the velocity vector $\mathbf{v}$, velocity gradient $\nabla\mathbf{v}$, and director $\mathbf{n}$ in the case of measuring the Miesowicz viscosity coefficients $\eta_1, \eta_2, \eta_3, \eta_{12}$.

at the pipe ends, we assume that the director forms an angle with the stream direction constant over the pipe profile. Let the director $\mathbf{n}$ lie in the shear plane and have a steady orientation (in the absence of turbulence). Then, the director alignment angle θ_0 at a high NLC flow velocity is given by the following expressions [6, 7]:

$$\cos 2\theta_0 = -\frac{\gamma_1}{\gamma_2} \quad\text{or}\quad \tan^2\theta_0 = \frac{\alpha_3}{\alpha_2} = \frac{\gamma_2+\gamma_1}{\gamma_2-\gamma_1}\,. \tag{3.3}$$

The Poiseuille flow becomes unstable if the coefficients α_3 and α_2 are opposite in sign. For example, as the NLC temperature is changed toward the smectic A phase, the coefficient α_3 changes sign and becomes positive. Then, the laminar flow turns to a turbulent one.

Ref. [8] proposes an analogy between the coefficients γ_1 and γ_2 and the thermodynamic parameters of a normal liquid.

Since the increase in entropy for a slow-changing perturbation is

$$\delta\dot{s} = \left(\frac{\partial s}{\partial T}\right)_\rho \delta\dot{T} + \left(\frac{\partial s}{\partial\rho}\right)_T \delta\dot{\rho}\,, \tag{3.4}$$

the use of the energy-conservation equation

$$T\,\mathrm{d}s + \frac{P}{\rho^2}\,\mathrm{d}\rho = \mathrm{d}\,\frac{\varepsilon}{\rho}\,,$$

the continuity equation $\dot{\rho} = -\nabla_i v_i$, and the equation of thermal conduction $\dot{T} = (\varkappa/\rho c_p)\nabla^2 T$ leads to the equation

$$\varkappa^{-1}T\rho\delta\dot{s} - \left(\frac{\partial P}{\partial T}\right)_\rho \varkappa^{-1}\nabla_i\delta v_i = \left(\frac{c_V}{c_p}\right)\nabla^2\delta T\,, \tag{3.5}$$

where P is the pressure, ε is the energy, ρ is the density, $\varkappa$ is the thermal conductivity, and c_V and c_p are the specific heat capacities at constant volume and pressure, respectively. The designation

$$\varkappa^{-1}T\rho = \bar{\gamma}_1\,,\qquad \left(\frac{\partial P}{\partial T}\right)_\rho \varkappa^{-1}T = \bar{\gamma}_2\,,$$

yields an equation identical in form to the equation for the director (2.16). This means that $\bar{\gamma}_1^{-1}$ is the Onsager transport coefficient, while $\bar{\gamma}_2$ is not. Thus, the propagation frequency

of the temperature mode is $\bar{\gamma}_1^{-1}\ (c_V/T)^{-1}$, i.e. the relationship between the parameters $\bar{\gamma}_1^{-1}$ and γ_1^{-1} implies a similar relationship between c_V/T and K_{ii}^{-1} (K_{ii} is the Frank elastic constant) and also between $(\mathrm{d}P/\mathrm{d}T)_\rho$ and $(1-\gamma_2)/\gamma_1$.

The difference between $\bar{\gamma}_1$, $\bar{\gamma}_2$, and γ_1, γ_2 is manifest as differences between hydrodynamic modes. For example, the Kubo formula cannot be written for γ_1 and γ_2, whereas it has the following form for γ_1^{-1}:

$$\gamma_1^{-1} = \lim_{\omega\to 0}\lim_{\mathbf{q}\to 0}\left(\frac{\omega^2}{2k_\mathrm{B}T}\right)S_{n,n}(\mathbf{q},\omega)\,, \tag{3.6}$$

where ω and $\mathbf{q}$ are the frequency and the spatial wave vector of the external perturbation (of the field), respectively. Without going into detail as regards expression (3.6), let us note that, throughout this review, the coefficients of viscosity are assumed to be measured at low temporal and spatial frequencies. Both the cell sizes and control regimes considered below are in line with this condition.

The relationship between nonhydrodynamic processes (coefficient of translational self-diffusion D) and viscosity η is described by the Stokes law

$$D \sim \frac{k_\mathrm{B}T}{6\pi\eta a}\,, \tag{3.7}$$

where a is the molecular size.

A similar expression can be obtained for the spatial orientation of a molecule by relating the coefficients of rotational diffusion D_rot and viscosity:

$$D_\mathrm{rot} \approx \frac{k_\mathrm{B}T}{\gamma_1 a^3}\,. \tag{3.8}$$

The relationship between these quantities has been used in [18] to derive the temperature dependence of rotational viscosity.

The equations of motion for different experimental geometries derived from (2.15) and (3.1) will be given below. The coefficient of LC rotational viscosity describes only the rate of director rotation and therefore has no analogue in an isotropic liquid. It should be noted from the very beginning that a phenomenon inverse to the director orientation due to the NLC flow exists — the so-called backflow, or hydrodynamic motion of a liquid crystal induced (under certain conditions) by the reorientation of the director under the action of an external field [19]. These two phenomena are directly related to the anisotropic structure of LC molecules, which is responsible for the difference between the coefficients α_3 and α_2 ($|\alpha_3| \ll |\alpha_2|$) and, therefore, for the torque difference corresponding to different director orientations [20]. The backflow accounts for the decrease in the coefficient γ_1 [20, 21] (see Section 7 for a detailed discussion). Splay elastic deformation is characterized by the quantity $\eta_S = \gamma_1 - \alpha_3^2/\eta_1$ and bend deformation by $\eta_B = \gamma_1 - \alpha_2^2/\eta_2$.

The temperature dependences of the Leslie (α_i) and Miesowicz η_i ($i = 1, 2, 3$) coefficients of viscosity and the rotational viscosity coefficient γ_1 for pentylcyanobiphenyl (BF-5) have been reported in [22–25] (see Fig. 2 for η_i and γ_1). Although the viscosities η_i and γ_1 describe dissipative processes differing in nature (shear flow and director rotation), they have interrelated values. It has been shown in [26] that the ratio $\eta/(\gamma_1 S^{-2})$, where η is the dynamic viscosity measured in a capillary LC flow (see Section 4 for details), is

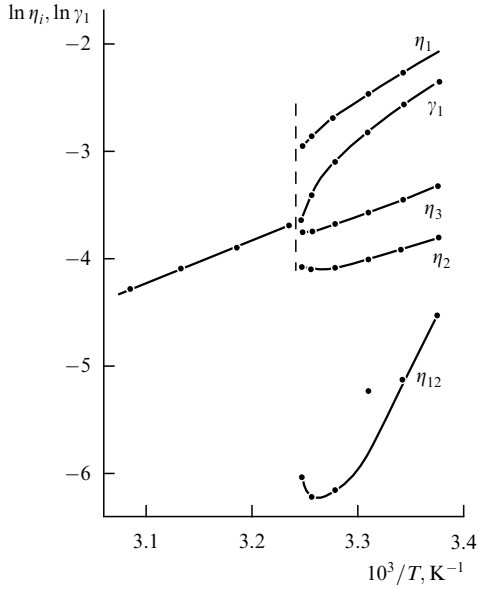

Figure 2. Temperature dependences of the Miesowicz viscosity coefficients η_1, η_2, η_3, η_{12} and rotational viscosity γ_1 for pentylcyanobiphenyl (BF-5) [23, 24].

virtually independent of temperature, being determined by the molecular structure of the substance. Barring a small interval near the clearing point, this ratio is virtually constant and determined by the structure of the NLC molecules.

An ample substantiation of the relationship between shear flow and NLC reorientation is presented in [27] where the identity

$$\frac{\eta_1}{\eta_2} \equiv \frac{\eta_S}{\eta_B}\,. \tag{3.9}$$

is proved. This identity can be used to characterize an NLC flow based on the measured coefficients of viscosity related to director deformation or to predict the reorientation velocity of the director from the capillary viscosity.

To summarize the foregoing in the context of the techniques of measuring the NLC viscosity, we note that, since all nematics are liquid, virtually any method used to deal with simple fluids (e.g. out of the methods listed in [28]) is suitable for the purpose. The most widespread (by virtue of their simplicity) methods are those which involve measuring the time of NLC passage through a capillary at a given shear rate. It has been shown that, owing to anisotropy, the measured viscosity is sensitive to a large number of variables, which are not always taken into account in routine viscometry. These are the shear velocity, the orientation of molecules at the tube wall, and external magnetic and electric fields, whose variations alter the effective viscosity due to reorientation of molecules in the flow. The flow may lose uniformity even at very low shear rates, for certain relations between the Leslie coefficients. At the same time, the NLC anisotropic properties make it possible to use alternative methods for the evaluation of viscosity, e.g. various optical and capacitance techniques. Viscosity is the complex component of the shear modulus; therefore, it can be measured by ultrasonic methods. The anisotropy of ultrasound propagation and absorption is responsible for the difference between the viscosity values obtained by ultrasonic and capillary flow techniques. Akin to the former is the method of determining

NLC viscosity coefficients by measuring the spectra of inelastic light scattering from surface waves.

A specific feature of liquid crystals is the development of viscous stresses in the absence of any flow, as the result of director reorientation due to changes in the direction or amplitude of the magnetic or electric field applied to the given nematic specimen. The viscoelastic ratio influences the relaxation time of thermal fluctuations of the director. Measurement of the Rayleigh light scattering spectrum intensity yields the set of NLC viscosity coefficients.

In what follows, we provide a detailed description of experimental conditions for the measurement of NLC viscosity coefficients, discuss their dependence on selected variables, and evaluate the accuracy of measuring techniques.

4. Shear flow technique

Since, by definition, the viscosity is the ratio of the applied shear stress to the shear deformation rate, it can be estimated by measuring the time of passage of a given LC volume through a capillary tube for a given pressure difference conditioned, e.g., by the fluid weight. The measured effective viscosity values strongly depend on the experimental conditions because of the viscosity anisotropy, the director orientation by the flow, and the interaction with the capillary walls.

The anisotropy of NLC viscosity was first observed by Miesowicz [17, 29] and Tsvetkov and Mikhailov [30]. The experiment of Miesowicz is described here based on his paper [31] using notation for η_i as in Figs 2 and 3. Miesowicz measured the damping of oscillations of a thin glass plate, 32×22 mm^2 in size, submerged in a liquid crystal. The plate was suspended from one arm of an analytical balance by a thin glass thread, 0.1 mm in diameter (Fig. 3a). The weight and shape of the plate were chosen so as to minimize the irregular movements of the plate due to thermal streams in the liquid. The small amplitude (3 mm) and rather long period (5 s) of oscillations ensured an extremely low velocity gradient. The plate was placed in a 6 mm thick rectangular vessel heated by an oil thermostat. A change in the angle φ between the magnetic field **H** and the normal to the plate (Fig. 3b) resulted in a change in the NLC viscosity, according to the law

$$\eta(\varphi) = \eta_1 \cos^2 \varphi + \eta_3 \sin^2 \varphi \,.$$

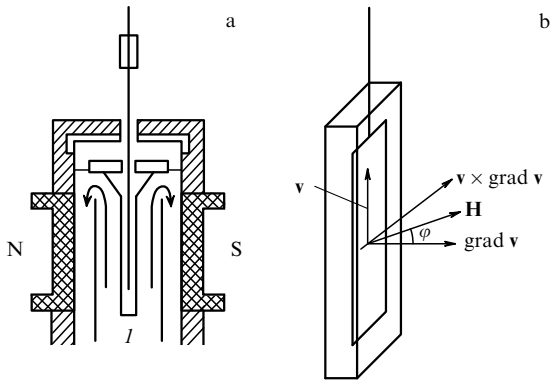

Figure 3. Apparatus used for the measurement of NLC viscosity coefficients from the damping of oscillations of a thin glass plate submerged in container *1* with NLC (a) and the position of the plate in container *1* relative to the velocity vectors, velocity gradient, and magnetic field (b) [31].

The value of **H** was chosen so as to exclude variations in the measured viscosity coefficient η_{eff} with subsequent increases in the magnetic field intensity. The quantity η_2 was measured in the absence of a magnetic field in the NLC capillary flow on the assumption that the director is completely reoriented by the flow. However, this was not exactly the case, as will be shown below.

This method was improved in [32], where the main difficulty, i.e. measuring the damped oscillation amplitude, was overcome. A beam of laser light was incident on a photodetector after passing through two diffraction gratings with a period of 10 μm. One of them was immovable while the other was connected to an oscillating plate. The plate oscillations can be described by the equation

$$\frac{\mathrm{d}^2 z}{\mathrm{d}t^2} + 2\beta \frac{\mathrm{d}z}{\mathrm{d}t} + \omega_0^2 z = 0 \,, \tag{4.1}$$

where ω_0 is the free oscillation frequency and β is a parameter proportional to the NLC viscosity. The solution of (4.1) is the function

$$z(t) = A \exp(-\beta t) \cos(\omega t + \phi) \tag{4.2}$$

for $\omega_0^2 > \beta^2$ (which is true for low-viscosity samples [in [32] $\eta < 2$ P)] and

$$z(t) = A_1 \exp\left[-(\beta - \delta)t\right] + A_2 \exp\left[-(\beta + \delta)t\right], \tag{4.3}$$

for $\omega_0^2 < \beta^2$. In (4.2) and (4.3), ϕ is the oscillation phase, $\delta = (\beta^2 - \omega_0^2)^{1/2}$, and $\omega = (\omega_0^2 - \beta^2)^{1/2}$. In [32], the amplitude of free oscillations was about 2 mm at a period of 14 s.

Unlike the experiment of Miesowicz, that of Tsvetkov and Mikhailov [30] was designed to measure viscosity variations caused by the applied magnetic field is an NLC capillary flow. This method was further developed in [16, 24, 33, 34]. Kneppe and Schneider [24] described an experimental setup and measuring procedure which gave very precise viscosity values. A schematic sketch of their apparatus is presented in Fig. 4. A capillary tube K positioned between the poles of a magnet is connected at each end to a closed vessel filled with nitrogen. An elevation of the pressure in one vessel induces an LC flow through the capillary. The pressure difference between the nitrogen-filled vessels is measured with an electronic manometer and printed out as a function of time at constant intervals controlled by a pulse generator. Approximation formulas are used to calculate the effective viscosity coefficient of the fluid η_{eff}, which is related through the experimental conditions to the measured Miesowicz viscosity coefficient η_i. The accuracy of measurements is improved by virtue of good LC orientation achieved by the use of a strong magnetic field, low shear rates, and a thick capillary tube with a wide longitudinal section. The capillary consists of 20 plates assembled together parallel (for measuring η_2, η_3) or normal (for measuring η_1) to the magnetic field, as shown in Fig. 4. The plates are made of a nonmagnetic metal (brass). The cross section of the capillary is 0.3×16 mm^2 and the total length amounts to 855 mm. These dimensions are significantly different from those used in [16] (0.4×50 mm^2) and [33, 34] ($0.3 \times 4 \times 50$ mm^3). In order to reduce the effect of LC surface tension, the inlet and outlet of the capillary block are connected to two glass cylinders C_1 and C_2 (15 mm inner diameter) for the storage of LC. Complete wetting is achieved by coating the inner

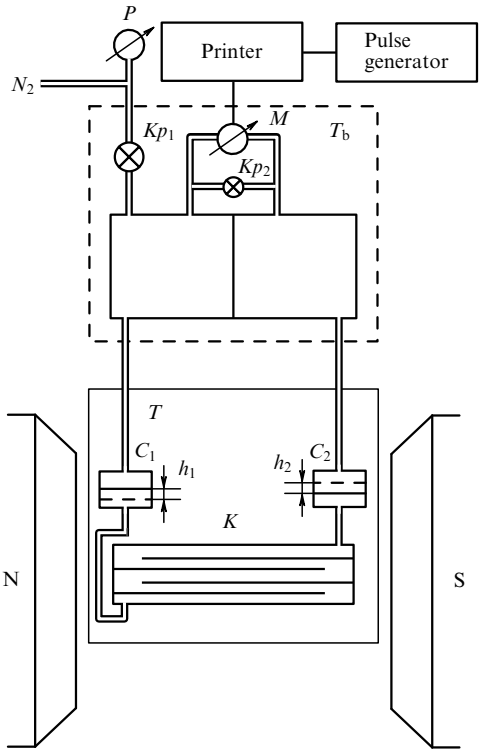

Figure 4. Experimental setup for measuring the coefficients η_1, η_2, η_3, η_{12} [24].

surface of the glass cylinders with a thin film of tin oxide. Bearing in mind the pressure dependence of the buffer gas compressibility, a constant nitrogen pressure is chosen for all measurements. In order to achieve an isothermal expansion of the buffer gas during the measurement, each buffer volume (85 cm^3 of N_2) consists of 25 boreholes of 7 mm diameter in the copper block. The capillary block, the glass cylinders C_1 and C_2, and part of the brass tubes connecting the cylinders to the buffer volumes are submerged in an oil bath, where the measurement temperature T can be controlled to within ± 0.01 K. The remaining part of the tubes, the buffer volumes, and the differential pressure manometer are placed in an aluminium case the temperature of which is maintained at the level $T_b = 22\,^\circ C$.

For a laminar flow in a long capillary, the flow rate of a liquid volume $\dot{V}$ with the coefficient of viscosity η is related to the pressure difference between the capillary ends through the expression

$$\dot{V} \sim \frac{\Delta p_c}{\eta} . \tag{4.4}$$

If the buffer gas assumed to be ideal and the diaphragm displacement in the manometer is proportional to the applied pressure difference Δp, the flow rate is proportional to the derivative of the gas pressure difference Δp with respect to time:

$$X \frac{d\Delta p}{dt} \sim -\frac{\Delta p_c}{\eta} , \tag{4.5}$$

where X is a factor dependent on the temperatures T and T_b, gas volumes, and diaphragm displacement. The difference between Δp and Δp_c is the hydrostatic pressure difference $\rho g \Delta h$ ($\Delta h = h_2 - h_1$):

$$\Delta p_c = \Delta p - \rho g \Delta h = \Delta p - (\Delta p_0 - \Delta p) A X \rho g . \tag{4.6}$$

Here, Δp_0 is the initial gas pressure difference (at $t = 0$ and $\Delta h = 0$) and A is a constant dependent on the cross section of cylinders C_1 and C_2. This allows (4.5) to be written in a form convenient for integration:

$$\frac{d\Delta p_c}{dt} = -\frac{K}{\eta X}(1 + AX\rho g)\Delta p_c , \tag{4.7}$$

where the constant K is determined by calibrating the viscometer with a standard liquid of a known η. However, expression (4.7) gives only the effective viscosity coefficient η_{eff}, which is lower than the corresponding Miesowicz coefficient of viscosity η_i because of the pressure gradient in the capillary. The fluidities (reciprocals of the viscosities) ϕ_{eff} and ϕ_i are related by the expression

$$\phi_{eff} = \phi_i + D\Delta p_c^2 \ (\eta_{eff}^{-1} = \eta_i^{-1} + D\Delta p_c^2) . \tag{4.8}$$

This expression, upon substituting it into (4.7) and subsequent integration, gives

$$\ln\left[\Delta p_c (1 + D\eta_i \Delta p_c^2)^{-1/2}\right] = -\frac{K}{\eta_i X}(1 + AX\rho g)t + C . \tag{4.9}$$

Although the coefficient D is a function of the experimental conditions and NLC viscosity coefficients, it is adjusted so as to obtain the maximum correlation coefficient for the experimentally found dependence $\Delta p(t)$, which is related to Δp_c by expression (4.6).

The relationship between η_{eff} and η_i can be derived from the equations of motion and orientation, which appear in the Leslie–Ericksen theory. We omit here the derivation procedure and present the principal results. The variation of the director tilt angle over the depth of the LC slab for the director and the velocity gradient parallel to each other (measurement of η_i, geometry 1 in Fig. 1) is described by the expression

$$\theta = \frac{\pi}{2} + \frac{\alpha_2 \mu_0}{\eta_1 \chi_a B^2} \frac{dp}{dz} = \frac{\pi}{2} + \beta_i x , \tag{4.10}$$

where $-a/2 < x < a/2$, a is the capillary thickness, χ_a is the diamagnetic anisotropy, B is the magnetic induction, and dp/dz is the pressure gradient along the capillary tube. The profile and mean value of the flow velocity $v(x)$ are described by the formulas

$$v(x) = \frac{1}{2\eta_1} \frac{dp}{dz}\left[x^2 - \frac{a^2}{4} + \frac{\beta_1^2}{6}\left(x^4 - \frac{a^4}{16}\right)\right] , \tag{4.11}$$

$$\langle v \rangle = -\frac{a^2}{12\eta_1} \frac{dp}{dz}\left(1 + \frac{\beta_1 a^2}{20}\right) , \tag{4.12}$$

and the effective viscosity η_{eff} by

$$\eta_{eff}^{-1} = \eta_1^{-1}\left(1 + \frac{\beta_1 a^2}{20}\right) . \tag{4.13}$$

If η_2 is measured in the presence of a magnetic field (velocity v is parallel to the director, geometry 2 in Fig. 1),

the director alignment angle is described by the expression

$$\theta = -\frac{\alpha_3 \mu_0}{\eta_2 \chi_a B^2} \frac{\mathrm{d}p}{\mathrm{d}z} . \tag{4.14}$$

It should be recalled that the quantity θ is determined by (4.7) in the absence of a field. In this case, the mean flow velocity is

$$\langle v \rangle = -\frac{a^2}{12\eta_2} \frac{\mathrm{d}p}{\mathrm{d}z} \left[1 - \frac{\beta_2 a^2}{20\eta_2} \left(\frac{\eta_1}{\eta_2} - 1 \right) \right] , \tag{4.15}$$

and the effective velocity is

$$\eta_{\mathrm{eff}}^{-1} = \eta_2^{-1} - \frac{\beta_2 a^2}{20\eta_2} \left(\frac{\eta_1}{\eta_2} - 1 \right) . \tag{4.16}$$

When the director is perpendicular to both the velocity and the velocity gradient, $\eta_{\mathrm{eff}} = \eta_3$. Therefore, pressure gradients are responsible for the underestimation of η_1 and η_2.

Another source of errors is associated with the boundary layers at the tube walls, whose width is

$$\xi = \sqrt{\frac{K_{ii}}{\chi_a \mu_0 H^2}} \cong \sqrt{\frac{K_{ii}}{\chi_a \mu_0 B^2}} , \tag{4.17}$$

and which are not oriented by the magnetic field (K_{ii} is the coefficient of elasticity). The Poiseuille flow near the walls and in the bulk of the cell has different profiles, which accounts for the dependence of η_i^{eff} on the magnetic coherence length ξ:

$$\frac{1}{\eta_i^{\mathrm{eff}}} = \frac{1}{\eta_i} + \left[6\frac{\xi}{a} - 12\left(\frac{\xi}{a}\right)^2 + 8\left(\frac{\xi}{a}\right)^3 \right] \left(\frac{1}{\eta_S} - \frac{1}{\eta_i} \right) , \tag{4.18}$$

where η_S is the coefficient of viscosity at the inner capillary surface. Neglecting the terms $(\xi/a)^2$ and $(\xi/a)^3$ and taking into account (4.17) leads to

$$\frac{1}{\eta_i^{\mathrm{eff}}} = \frac{1}{\eta_i} + \sqrt{\frac{K_{ii}\mu_0}{\chi_a}} \frac{6}{aB} \left(\frac{1}{\eta_S} - \frac{1}{\eta_i} \right) . \tag{4.19}$$

Thus, the Miesowicz coefficient of viscosity η_i can be obtained by the extrapolation of the dependence η_{eff}^{-1} on B^{-1} to infinitely large values of magnetic induction (Fig. 5). It follows from Fig. 5 that the measured η_2 and η_3 values are close to true real ones in sufficiently intense fields. Nevertheless, even at $B = 1.1$ T the measurement error is as large as 10%. This fact and the high shear rates seem to explain the underestimation of the η_1 values by Gaehwiller [16]. On the other hand, the viscosity coefficients η_1 reported by Miesowicz [29, 31] are correct because they were measured in a thick (6 mm) sample at low shear rates.

Effects of the director orientation at the wall of a capillary tube were studied in [35]. If the orientation is controlled only by the magnetic field, the effective coefficient η_1 is proportional to B^{-1} and its true value can be obtained by extrapolation for $B^{-1} \to 0$. If a nematic contains an admixture of 0.1% cetyltrimethylammonium bromide (CTAB), which facilitates its homeotropic orientation in a plane capillary, then $\eta_1^{\mathrm{eff}} = \eta_1$ for a magnetic field $B < 1.1$ T and a pressure difference of 100 Pa between the capillary ends (see Fig. 5). The flow profile also depends on the size of the aperture. If it is much smaller than the capillary width, the inflowing LC moves more slowly near the wall than in the bulk of the capillary. As a result, the tangent to the front edge

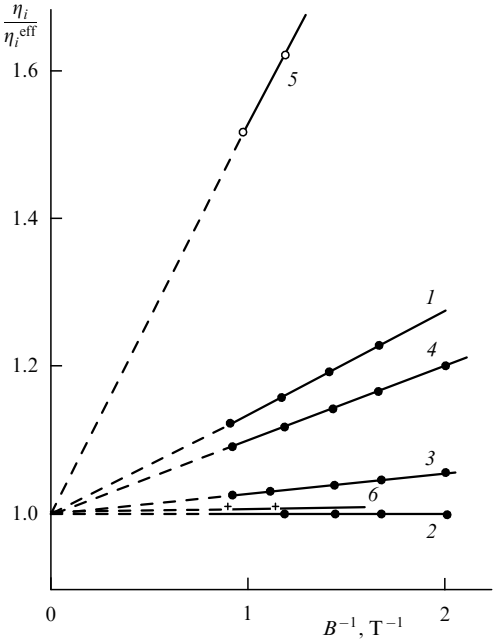

Figure 5. The quantity η_i^{eff} ($\eta_i/\eta_i^{\mathrm{eff}}$ ratio) as a function of the magnetic field B in the measurements of η_1 (*1*), η_2 (*2*), η_3 (*3*), η_{12} (*4*) for MBBA [24] and η_1 (*5*, *6*) for dibutylazoxybenzene (DIBAB) [35]. (*1*, *5*) $\eta_i/\eta_i^{\mathrm{eff}}$ values obtained without previous treatment of the capillary surface; (*6*) DIBAB with 0.1% cetyltrimethylammonium bromide added to maintain homeotropic orientation.

of the inflowing LC makes different angles ($+\alpha$ and $-\alpha$) with the long capillary axis. In the front region, the LC turns in different directions with respect to the flow alignment. In a twisted nematic cell, this results in the appearance of domains subject to differently directed torques [36].

Effects of boundary conditions on the Couette flow of a molecular liquid are studied theoretically in [37]. Let a liquid crystal be sandwiched between two plates moving in the y-direction at velocities v_s and $-v_s$ and situated at distances L and $-L$ from the center of the layer. The no-slip boundary conditions for the derivative of the orientational part of the free energy $k_B T$ with respect to the orientation tensor $a_{\mu\nu}$ can be written as

$$\Sigma_{\mu\nu} = \frac{\partial \Sigma}{\partial a_{\mu\nu}} = A a_{\mu\nu} = C_{am} (n k_B T)^{-1} k_\mu^{\tan} n_\nu + C_a C_0^{-1} n_\lambda b_{\lambda\mu\nu} . \tag{4.20}$$

Here, $C_0 = (k_B T/m)^{1/2}$ is the thermal velocity of a molecule of mass m, n_ν is the component of the unit vector normal to the liquid surface, $k_\mu = n_\nu \bar{P}_{\mu\nu}$, $P_{\mu\nu}$ is the component of the friction pressure tensor, $b_{\lambda\mu\nu} = D_a \nabla_\lambda a_{\mu\nu}$, and D_a is the coefficient of rotational diffusion. The overbar denotes the symmetric traceless part of the tensor, e.g.

$$\bar{a}_\mu \bar{b}_\nu = \frac{1}{2}(a_\mu b_\nu + a_\nu b_\mu) - \frac{1}{3} a_\lambda b_\lambda \delta_{\mu\nu} .$$

The index 'tan' stands for the tangential vector component, e.g. $k_\mu^{\tan} = k_\mu - n_\mu n_\nu k_\nu$. The surface is characterized by the dimensionless coefficient $C_a \geqslant 0$ that describes the orientation. The effective viscosity coefficient η_{eff} can be found from the condition

$$p_{xy}(L) = -\frac{\eta_{\mathrm{eff}} v_s}{L} . \tag{4.21}$$

However, the true velocity gradient γ_0 differs from the measured one, $\gamma = v_s/L$, and can be written using functions related to the surface orientation:

$$\gamma_0 = \frac{Rv_s}{L}; \quad R^{-1} = \left\{1 + Q\frac{l}{L}\tanh\frac{L}{l}\left[1 + \beta\tanh\frac{L}{l}\right]^{-1}\right\}, \tag{4.22}$$

where the quantity Q is related to the ratio of viscosity coefficients at low and high shear rates (η and η_∞, respectively), being a combination of relaxation times that describe translational ($\eta = nk_BT\tau_p$) and rotational ($\gamma_1 = 3nk_BTS^2\tau_a$) motions of the director and its torsion ($\gamma_2 = 2 \times 3^{1/2}\, nk_BTS\tau_{ap}$; $\tau_{ap} = \tau_{pa}$, according to the Onsager relation):

$$Q = \frac{\eta}{\eta_\infty} - 1 = \frac{\tau_{ap}\tau_{pa}}{\tau_a\tau_p}\left(1 - \frac{\tau_{ap}\tau_{pa}}{\tau_a\tau_p}\right)^{-1}; \tag{4.23}$$

l is related to the characteristic length l_a (the scale of variations in a spatially nonuniform orientation; $l_a^2 = D_a\tau_a$) by the expression

$$l^2 = \left(1 - \frac{\tau_{ap}\tau_{pa}}{\tau_a\tau_p}\right)l_a^2. \tag{4.24}$$

It can easily be seen that $\tau_{ap}\tau_{pa}/\tau_a\tau_p = \gamma_1\eta/4\gamma_2^2$. Then, $l \approx 0.96\, l_a$, $Q \sim 0.1$ if $|\gamma_2| \approx \gamma_1 \approx 3\eta$. The maximum possible Q value for typical NLCs obtained from the relaxation time ratios (or corresponding viscosity ratios) is 0.33 at $|\gamma_2| \approx \gamma_1 \approx \eta$, i.e. $(\eta/\eta_\infty)_{max} = 1.33$. Generally speaking, this value is somewhat smaller than the actual variation of the effective η value in a flow ($\eta_1/\eta_2 \approx 3$).

Only the parameter β in (4.22) is directly related to the surface orientation:

$$\beta = C_aD_a(C_0l)^{-1}. \tag{4.25}$$

The parameter R differs from unity because the velocity profile of the Couette flow at a small β differs substantially from a linear one and is described by the expression

$$v_x = Rv_s\left[\frac{y}{L} + Q\frac{l}{L}\cosh\frac{L}{l} + \beta\sinh\frac{L}{l}\sinh\frac{y}{L}\right]^{-1}. \tag{4.26}$$

At low β or L/l and near the plates, the director undergoes an incomplete orientation by the flow. This increases the measured viscosity, described by (4.21). The following relation, obtained from (4.22), is satisfied if the distance between the plates is sufficiently large ($L > 4l$):

$$\frac{\eta}{\eta_{eff}} - 1 \approx Ql(1 + \beta)^{-1}. \tag{4.27}$$

It was shown in [38] that not only the inclination of the director, described by (3.3), but also its torsion is possible for certain boundary conditions and shear stresses. Under planar or homeotropic boundary conditions, the reorientation of the director usually takes place in the x, y plane formed by the director and flow velocity vectors. However, if the orientation is tilted against the flow, the LC layer can experience a torsional strain under a shear stress exceeding the threshold value.

Let us denote the viscosity coefficient measured in a capillary NLC flow at high shear rates by η_c. In early experiments [16, 24, 29, 33], η_c was considered equal to η_2. If we assume that, in a capillary flow, the director alignment angle relative to the velocity vector tends to a saturation value (zero), we shall have for η_c [39]

$$\eta_c = 0.25\alpha_2\left(1 - \frac{\gamma_1^2}{\gamma_2^2}\right) + 0.5(\alpha_2 + \alpha_4 + \alpha_5). \tag{4.28}$$

The difference between η_c and η_2 [see (3.1)] is

$$\Delta\eta_c = \eta_c - \eta_2 = -\alpha_3\left(1 + \frac{\alpha_1\alpha_2}{\gamma_2^2}\right), \tag{4.29}$$

very small for most NLCs.

The measured η_c strongly depends on the capillary radius and shear rate. Figure 6 shows the temperature dependences of the apparent (i.e. effective, experimentally measured) viscosity η_{eff} in capillary tubes of three different inner radii (175, 335, and 452 μm) [40]. At the same shear rate, the apparent viscosity for the smaller tube is 10% higher than that for the larger tube.

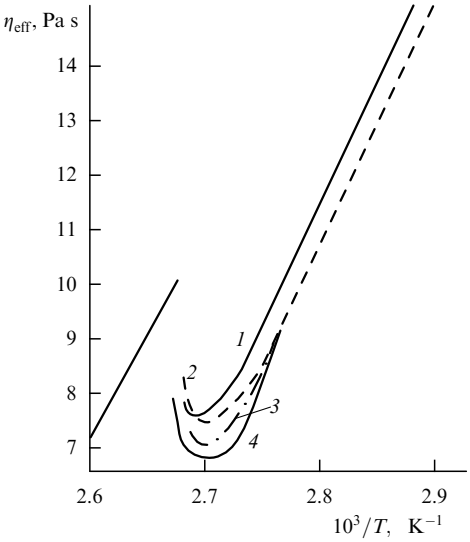

Figure 6. Temperature dependence of the viscosity coefficient for hexyloxybenzylidene aminobenzonitrile (HBAB) measured in capillary tubes of inner radius 175 μm (*1*), 335 μm (*2*), and 452 μm (*3*) and by the falling ball technique (*4*) at a mean gap of 1400 μm between the ball and the tube walls [40].

A similar effect is observed if the shear velocity is varied without changes in the capillary size. Ref. [41] describes a method for measuring the viscosity of an NLC in the gap between concentric circular cylinders rotating with different angular velocities. The dependence $\eta_{eff}(\gamma)$ for a wide range of γ values can be described by the relation

$$\eta_{eff} = \eta_2 + b|\gamma|^{-1} = \eta_2 + bG, \tag{4.30}$$

where $G = |\gamma|^{-1}$. This dependence reaches a saturation at shear rates above 2000 s^{-1} (para-azoxyanisole, $t = 120\,^\circ$C). For a homeotropic orientation of the LC at the surfaces of the cylinders and low shear rates, $\eta_{eff} \to \eta_1$ [41]. It is also shown in [41] that heat fluxes in the flow do not appreciably affect the director orientation.

The capillary-radius and shear-velocity dependences arise from the influence of these parameters on the pressure

gradient along the capillary, $q = \mathrm{d}p/\mathrm{d}z$. In the general case, the viscosity η_c is described by the relation

$$\eta_c = \frac{\pi q R^4}{8Q}\,, \tag{4.31}$$

where $Q = 2\pi\int_0^R v(r) r\,\mathrm{d}r$ is the LC volumetric flow rate. By constructing dependences of η_c on the Atkin number $4Q/\pi R$ (which is a single-valued function of the product qR^3 in the absence of an electric or magnetic field [42, 43]), it is possible to find such values of the capillary radius and shear velocity at which these parameters cease to influence the apparent viscosity. It follows from Fig. 7a that the effective viscosity is virtually independent of the capillary radius if $R > 300$ μm. This corresponds to the Atkin number $4Q/\pi R = 0.1-0.2\,\mathrm{cm^2\,s^{-1}}$ and agrees with the data for para-azoxyanisole. The experimental findings of Fisher and Frederickson [44] for different capillary radii and shear rates are in good agreement with numerical solutions to the equations for the director continuity and variation in an NLC flow through a cylindrical capillary tube with homeotropic boundary conditions at its walls [45]. In the case of a well-established flow in the absence of a magnetic field, these equations have the form

$$2f(\theta)\frac{\mathrm{d}^2\theta}{\mathrm{d}r^2} + \frac{\mathrm{d}f}{\mathrm{d}\theta}\left(\frac{\mathrm{d}\theta}{\mathrm{d}r}\right)^2 + \frac{2f}{r}\frac{\mathrm{d}\theta}{\mathrm{d}r} - \frac{K_{11}\sin 2\theta}{r^2} + (\gamma_1 + \gamma_2\cos 2\theta)\frac{\mathrm{d}v}{\mathrm{d}r} = 0\,,$$

$$\frac{\mathrm{d}v}{\mathrm{d}r} = \frac{1}{g(\theta)}\left(-\frac{qr}{2} + \frac{b}{r}\right), \tag{4.32}$$

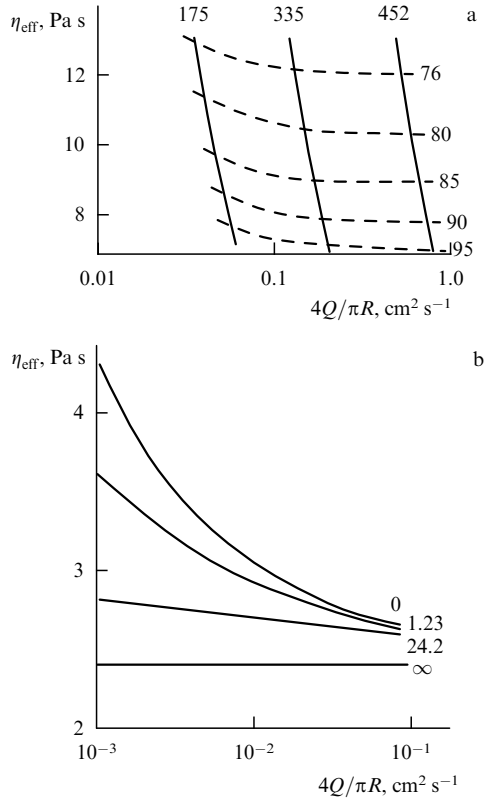

Figure 7. (a) Effective viscosity against the Atkin number (the ratio of the flow rate to the radius) $4Q/\pi R$ for different capillary radii [40] and (b) $\chi_a H^2$ [46]: (a) HBAB (dotted lines denote isotherms), (b) PAA.

where

$$f(\theta) = K_{11}\cos^2\theta + K_{33}\sin^2\theta\,,$$

$$g(\theta) = \alpha_1\sin^2\theta\cos^2\theta + (\alpha_5 - \alpha_2)\sin^2\theta + (\alpha_6 + \alpha_3)\cos^2\theta + \alpha_4\,, \qquad q = -\frac{\mathrm{d}p}{\mathrm{d}z}\,. \tag{4.33}$$

At $4Q/\pi R > 0.1$ cm^2 s^{-1}, both the theory and experiment confirm the existence of a well-established director orientation in a capillary NLC flow. However, there is no established orientation in highly viscous fluids (especially those containing smectic clusters) even at large Atkin numbers. If a magnetic field is imposed, the Atkin number at which the effective viscosity becomes saturated decreases. Figure 7b shows the results of a numerical calculation of $\eta_c(4Q/\pi R)$ for various $\chi_a H^2$ values [46].

In a capillary NLC flow with homeotropic boundary conditions at the walls, the influence of the boundaries is significant within a region of thickness δ.This quantity is determined by the expression

$$\frac{R-\delta}{R} = \frac{R_{cyl}}{R} = \frac{\eta_{cyl}}{\eta_w}\left(\frac{\eta_{eff}-\eta_w}{\eta_{eff}-\eta_{cyl}}\right)^{1/4}, \tag{4.34}$$

where R_{cyl} is the radius of the core region of the capillary in which the NLC undergoes realignment, η_{cyl} is the viscosity coefficient in this zone, and η_w is the viscosity coefficient in the boundary layers [44]. With $\eta_{cyl} = \eta_2$, $\eta_w = \eta_1$ and experimentally found viscosities, we obtain $R_{cyl}/R = 0.93-0.94$ for capillaries of different diameter, in agreement with microscopic observations of NLC flows [34].

According to [47], the viscosity increases with increasing mechanical stress, which is evidence for a highly regular structure of LC.

Various aspects of viscosity measurement in an NLC flow are also considered in [48]. If an NLC flows in a capillary tube under the gravity force alone (as in the Ostwald viscometer), the pressure difference between the tube ends is $\Delta p = \rho g h$, where h is the average height of the liquid and ρ is its density. The kinematic viscosity of a Newtonian fluid is described by the Poiseuille equation which establishes proportionality of viscosity to the passage time taking into account corrections for the kinetic energy effects [49]:

$$v = Ct + \frac{B}{t}\,, \quad C = \frac{\pi R^4 g h}{8LV}\,, \tag{4.35}$$

where L is the tube length and V is the volume of the flowing fluid. As a rule, the second term in (4.35) is neglected at $t > 200$ s, and the constant C is determined measuring the flow time of a fluid of known viscosity (with unknown h and V).

In the Ubbelohde viscometer, the gravity effect is compensated by the presence of the second arm of the capillary tube and the thorough adjustment of air pressure. Therefore, the capillary flow time is independent of the LC density and proportional to the dynamic viscosity η.

Ref. [50] describes a viscometer that makes it possible to measure the kinematic viscosity in a small NLC volume (0.4 – 0.6 ml). Even less LC is needed to measure the viscosity in the microviscometer developed in [51] on the basis of the microcapillary device described in [52]. This instrument consists of a 50 cm long, precision tube (of inner

diameter 0.2–0.4 mm) in which the temperature is maintained constant by a thermostat to within ±0.02 K. The fluid travels under the action of its own weight in the upright capillary tube. The displacement f the fluid level is recorded by a cathetomer. The amount of fluid needed to measure the viscosity (to an accuracy of 1%) may be as small as 50–100 mg because the capillary has no dilated cavity through which the fluid is introduced, in contrast to the capillary described in [50].

It has been mentioned above that in an NLC flowing through a capillary tube with homeotropic boundary conditions at a low shear rate, the director deviates from its initial orientation by an angle θ_0 determined by the ratio α_3/α_2 [or γ_1/γ_2, see (3.3)]. If the sign of α_3 changes from negative to positive, optical detection reveals a decrease of θ_0 to zero, the breakdown of the steady laminar flow into irregular domains, and the appearance of disclination lines parallel to the flow direction [5]. However, capacitance measurements reveal no peculiarities in the temperature dependence of angle θ_0 [53]. The last two studies investigated flows of hexyloxybenzylidene aminobenzonitrile ($C_6H_{13}O-C_6H_4-CH=N-C_6H_4-CN$, nematic range 56–101 °C, $t(\alpha_3 = 0) = 91$ °C). A detailed description of the experimental technique employed in [53] may be useful to understand this paradox. A brass cylinder is rotated with an angular velocity ω ($1\ \text{min}^{-1} < \omega/2\pi < 1\ \text{s}^{-1}$) inside a glass cylinder. Shielding electrodes are sealed in opposite walls of the glass cylinder together with measuring electrodes parallel to the cylinder axis. The capacitance of the LC volume placed between the short-circuited electrodes and the brass cylinder (second measuring electrode) is measured using a bridge. Evidently, the capacitance of the LC is a function of the director alignment angle. This system is subject to a magnetic field oriented so as to preserve the capacitance balance after the magnetic field is removed. The measurements are also made with the opposite direction of the cylinder rotation. The angle between the **H** directions thus found, corrected for the cylindrical configuration of the electrodes, is $2\theta_0$. Although a change in the sign of α_3 results in flow instability and the formation of inversion walls with a director alignment angle of $180° - 2\theta_0$, the measured capacitance remains unchanged. A hypothetical structure for the director orientation in an unstable flow is suggested in [40].

A nonuniform distribution of director orientations in a flowing LC layer can arise under the conditions described in [54]. If the director at the substrate plates is rigidly oriented at an angle θ_1, a constant shear stress τ_1 applied to one of the plates deforms the director in the bulk of the layer. A type-*1* or -*2* deformation may occur, depending on the relation $\theta_1 \gtrless \theta_0 = \arctan(\alpha_3/\alpha_2)$ [see (3.3)] (Fig. 8a). The director behavior in an LC layer at different shear stresses is in fact a solution to the Euler–Lagrange equation

$$K\frac{\mathrm{d}^2\theta}{\mathrm{d}z^2} = \tau\frac{\alpha_3\cos^2\theta - \alpha_2\sin^2\theta}{0.5(\alpha_3+\alpha_4+\alpha_6) - (\alpha_3+\alpha_2)\sin^2\theta}, \qquad (4.36)$$

where $K = (K_{11} + K_{22} + K_{33})/3$ is the mean elasticity coefficient. If $\theta_1 > -\theta_0$, the function $\theta_{\max}(\tau)$ tends to θ_0 as $\tau \to \infty$; if $\theta_1 < -\theta_0$, $\theta_{\max}(\tau) \to \theta_0 - \pi$ as $\tau \to \infty$. If $\theta_1 = -\theta_0$, a deformation threshold exists, and metastable states are possible. For a 10 μm thick MBBA layer, the threshold is about 0.1 N m^{-2}. A nonuniform distribution of director orientations may be responsible for distortions of the measured viscosity. The effective viscosity coefficient for the LC layer shown in Fig. 8a is described by the relation

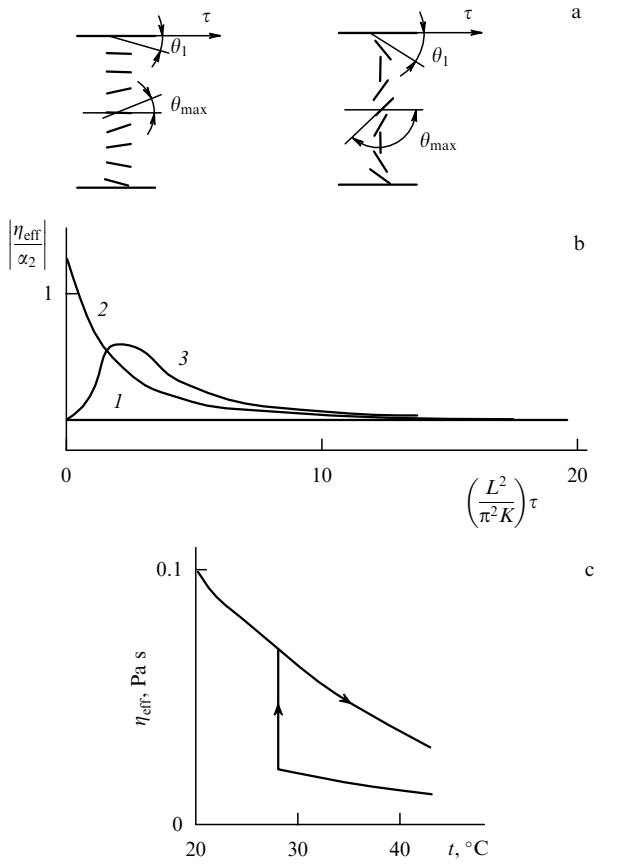

Figure 8. Feasible deformations in a shear flow [48] for different boundary conditions (a) and the dependence of effective viscosity η_{eff} on shear stress τ (b) and temperature (c) [48]: (b) *1*, $\theta_1 = \theta_0$; *2*, $\theta_1 = \pi/2$; *3*, $\theta_1 = -0.1$; $\alpha_3/\alpha_2 = 0.01$, $\eta_2/\alpha_2 = -0.2$; (c) $\theta_1 = 0.18$, $\tau = 3\pi^2K/L^2$.

$$\eta_{\text{eff}} = L\left\{\int_{-L/2}^{+L/2}\left[\eta_2 - (\alpha_3 - \alpha_2)\sin\theta\right]^{-1}\mathrm{d}z\right\}^{-1}. \qquad (4.37)$$

A nonmonotonic dependence $\theta(z)$ at $\theta_1 < -\theta_0$ can lead to a similar dependence of η_{eff} on the shear stress and to a bistable temperature dependence (Fig. 8b, c).

Under nonsymmetric boundary conditions (e.g. planar on one substrate plate and homeotropic on the other), the calculation of the time dependence of the LC reorientation must take into account the so-called surface viscosity [55]. The reader is referred to Refs [56–58] for a more detailed discussion of this problem. The surface viscosity dimension is that of the product of viscosity by the characteristic length (cell or boundary layer thickness). In [55], the surface viscosity is estimated to be 2.7×10^{-7} N cm^{-1}. If this viscosity is ignored, a 20-fold discrepancy arises between the surface energy values obtained in static and dynamic studies of the Freedericksz transition.

If static disclinations are present in a moving nematic, they may either attract or repulse the flow, depending on their strength [59] (Fig. 9). Certainly, this also leads to uncertainties in the measured viscosity. A case of disclination motion is considered below.

In the foregoing, we discussed the situations where the NLC viscosity was determined from the characteristic time

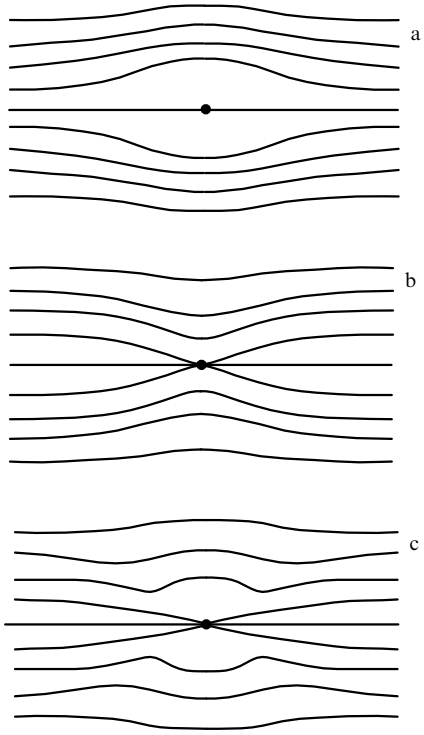

Figure 9. Distribution of NLC flow lines near linear disclinations of different strength: $S = +1$ (a), $S = -1$ (b), $S = -2$ (c) [59].

taken by a fluid volume to pass through a capillary tube. We also repeatedly noted that the flow influences the nematic orientation [relation (3.3)]. Since a nematic deformation entails significant changes in the optical characteristics of the nematic, optical methods of measuring the angle θ_0 are preferable.

In [16, 35], the director alignment angle θ_0 in a capillary NLC flow was obtained by an optical method from the optical path difference $\Delta\Gamma$ between the ordinary and extraordinary components of polarized light. At a certain (not very high) shear rate, $\theta(x)$ in the LC layer (with the exception of the transition layer) became a constant equal to θ_0 at $x > 0$ and $-\theta_0$ at $x < 0$. For small θ_0 values (almost invariably typical of experiment),

$$\Delta\Gamma = \int_{-L/2}^{L/2} \left[\frac{n_e n_o}{(n_e^2 \cos^2\theta + n_o^2 \sin^2\theta)^{1/2}} - n_o \right] dx = -\frac{1}{2} n_e L \frac{n_e^2 - n_o^2}{n_o^2} \sin^2\theta . \tag{4.38}$$

In [35], two branch pipes for inflowing and outflowing LC were cemented at the two ends of a plane capillary section. In [60], the measuring cell had a similar shape and was also used to study electrical conductivity and dielectric permittivity.

An original method of determining the director alignment angle (and hence, the γ_1/γ_2 ratio) from a single measurement over a wide range of shear velocities is described in [61]. The measuring cell consists of two circular glass plates, with a homeotropic orientation of the NLC at their surfaces. One plate is rotated at a constant angular velocity ω. A point at a distance r from the axis of rotation had the linear speed $v = \omega r$. Thus, a broad range of shear rates is covered (the angular velocity is varied from 4.19×10^{-5} to 4.19×10^{-2} s^{-1}). Since the flow alignment angle in the bulk of the sample increases with increasing v, the birefringence of the LC layer also varies, thus leading to the appearance of a system of light and dark concentric rings when the cell is illuminated by monochromatic light (in [61], $\lambda = 546$ nm). The ring number is related to the average birefringence at the distance r from the rotation axis via the expression

$$\frac{m\lambda}{L} = \langle n_e(r) - n_o \rangle , \tag{4.39}$$

where L is the thickness of the nematic layer which ranges between 40 and 500 μm and departs from the mean value by less than 2 μm. The radius r^* (or number m) at which the ring density is maximum (while the distance between rings is minimum) is determined to find the viscosity ratio. The ratio r^*/mL is a function of the NLC physical characteristics and temperature. The dependence of m/L on $(vL)^{-1/2}$ fit a straight line from the slope of which the γ_1/γ_2 ratio is deduced:

$$\frac{\gamma_1}{\gamma_2} = 1 - \frac{2(1 - w^{-2})}{(1 - n_e^2/n_o^2)} , \quad w = \frac{m}{L} \frac{\lambda}{n_e} + 1 . \tag{4.40}$$

To obtain the absolute values of the viscosity coefficients using this approach, the LC-should be placed in a magnetic [62] or electric [63, 64] field. In [64], the viscosity is determined from the optical characteristics of an LC layer confined between two rotating circular glass plates. It is shown that this method is applicable to NLCs with a positive as well as negative dielectric anisotropy. Unlike (4.40), the ratio of the ring number to the LC field thickness is a function of both the LC characteristics and the applied voltage. Therefore, the viscosity is determined from the coefficients by means of the approximation

$$\frac{m}{L(vL)^2} = a_1 + a_2 (vL)^2 , \tag{4.41}$$

$$a_1 = \frac{n_e}{960\lambda} \left(1 - \frac{n_e^2}{n_o^2} \right) \frac{(\gamma_1 - \gamma_2)^2}{K_{33}^2} \left[1 + \frac{\varepsilon_a U^2 (\gamma_1 - \gamma_2)}{8 K_{33}} \right]^{-2} \times \left[1 - \frac{17}{14} \frac{\varepsilon_a U^2}{8 K_{33} \eta_2} \left(4 - \frac{\gamma_1 - \gamma_2}{\eta_2} \right) \right] , \tag{4.42}$$

$$a_2 = \frac{n_e}{630} \left(1 - \frac{n_e^2}{n_o^2} \right) \frac{(\gamma_1 - \gamma_2)^4}{K_{33}} \left[1 + \frac{\varepsilon_a U^2 (\gamma_1 - \gamma_2)}{8 K_{33}} \right]^{-4} \times \left[\frac{36}{11} \frac{\varepsilon_a U^2}{K_{33} \eta_2} \left(4 - \frac{\gamma_1 - \gamma_2}{\eta_2} \right) - \frac{17(K_{33} - K_{11})}{K_{11}} - \frac{4}{3} \right] . \tag{4.43}$$

Expressions (4.41) – (4.43) were obtained for the conditions of a small director deformation in an NLC flow. In the case of zero field, $U = 0$, the ratios $(\gamma_1 - \gamma_2)/K_{33}$ and K_{33}/K_{11} can be derived. The values of K_{33}, K_{11}, $(\gamma_1 - \gamma_2)$, and η_2 can be found from approximations. At high shear rates, the ratio γ_1/γ_2 can be obtained using (4.40). This means that the method under consideration allows the absolute values of γ_1, γ_2, and η_2 to be determined. Ref. [64] puts a limit on the effective voltage applied to the LC layer. At $\varepsilon_a < 0$, the applied voltage must be smaller than $[48 K_{33} \eta_2 / |\varepsilon_a| (\gamma_1 - \gamma_2)]^{1/2}$. For MBBA, the limiting U value is 17 V and lies below the EGD-instability threshold at a sufficiently high frequency. A stricter limitation for NLCs with any sign of ε_a follows from the smallness of the displacement angle θ. If $\theta = \theta_{max}[1 + (\varepsilon - 1)4z^2/L^2]$,

where θ_{max} is the maximum displacement angle and ε is a small parameter, U must not exceed

$$U_1 = \left[\frac{8K_{33}\varepsilon}{|\varepsilon_a|(4-(\gamma_1-\gamma_2)\eta_2^{-1})}\right]^{1/2}.$$

For pentyl cyanobiphenyl, $U_1 \sim \varepsilon^{1/2}$ and equals 0.4 V at $\varepsilon \sim 1$. It is argued in [55] that the experiment may be carried out at a higher voltage. To verify this inference, it is necessary to obtain a numerical solution to the nonlinear equations that describe the NLC dynamics. This method is not widely used for measuring the NLC viscosity, but it has been successfully employed to measure the coefficients α_2 and α_3 of polymeric liquid crystals [65].

Although the above-described method allows one to determine a set of NLC viscosity coefficients, standard rotational viscometers, which consist of a flat plate and a rotating cone with the base radius R and cone angle $180-2\alpha$, are used much more widely [49, 66]. Such an instrument measures the moment acting on the plate. This technique is advantageous in that neither the voltage nor the shear velocity depends on R at small α.

The falling-ball technique is one more method used in viscometry. The coefficient of viscosity η_{FB} obtained by this method is smaller than that measured in a capillary NLC flow (see Fig. 6) and it is very close to the Miesowicz coefficient of viscosity η_2 [40]. The quantity η_{FB} does not depend on the width of the gap between the ball and the cylinder walls. It slightly increases in the temperature range where the coefficient α_3 changes its sign, probably due to the onset of turbulence [40]. The falling-ball technique is especially convenient in those experiments where a shear flow cannot be realized, e.g. in samples subject to high pressures [67, 68].

5. Ultrasonic methods for measuring the NLC viscosity

Coefficients of viscosity close to those in an NLC shear flow through a capillary tube can also be obtained by measuring ultrasonic shear waves propagating across a nematic layer [69, 70]. Depending on the mutual orientation of the director **n**, ultrasonic displacement **u**, and ultrasound wave vector **k** (Fig. 10), one of the three coefficients of viscosity can be determined:

$$\eta_A = \frac{\alpha_4}{2}, \quad \eta_B = \frac{1}{2}\left(\alpha_4+\alpha_6-\frac{\alpha_3\gamma_2}{\gamma_1}\right),$$

$$\eta_C = \frac{1}{2}\left(\alpha_4+\alpha_5-\frac{\alpha_2\gamma_2}{\gamma_1}\right). \qquad (5.1)$$

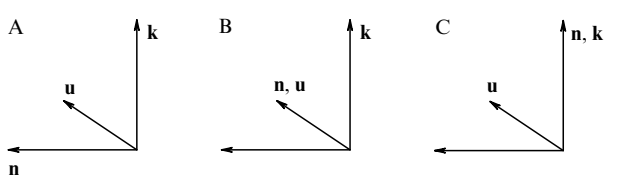

Figure 10. Relative positions of the ultrasonic displacement vector **u**, wave vector **k**, and director **n** in the measurement of viscosity coefficients η_A, η_B, η_C by ultrasonic methods.

It is easy to show that $\eta_B \equiv \eta_C$ (the Rapini equality). The quantity η_B differs from η_2 by

$$\Delta\eta_{B2} = \eta_B - \eta_2 = -\frac{1}{2}\alpha_3\left(1+\frac{\gamma_2}{\gamma_1}\right). \qquad (5.2)$$

Since $|\alpha_3|$ is small and $\gamma_2/\gamma_1 \approx -1$, the difference between η_B and η_2 turns out to be insignificant. It is worthwhile to mention that the coefficient η_B has a different set of Leslie coefficients and a different meaning compared to the bend viscosity coefficient, denoted by the same subscript (see Sections 7 and 8).

The ultrasonic methods used to measure the coefficients of viscosity η_A, η_B, and η_C are described at length in [70]. The pulse-phase method proposed in [69] for determining the NLC viscosity is based on the measurement of the amplitude and phase of the signal reflected from the surface of a measuring element on which the nematic layer is placed and oriented in a certain manner. The measuring element is a trapeziform plate of fused quartz to one end of which an ultrasound vibrator, also working as a receiver, is glued. An advantage of the pulse-phase method described in [69, 70] lies in the possibility of measuring the viscosity of a relatively small amount of LC (0.5–1 g) over a very wide range of values (10^{-3}–10^{12} Pa s). The drawbacks stem from the fact that the mechanical characteristics of the measuring element and gluing quality are strongly time- and temperature-dependent. Moreover, high reflection orders should be used to measure the reflection coefficients and phase shifts for low-viscosity liquids ($\eta < 0.1$ Pa s), which reduces the signal-to-noise ratio. The accuracy of the method is 5–10% (20% for low-viscosity liquids), and this method is unsuitable for express analysis.

The viscosity coefficients in the range 0.005–5 Pa s, typical of nematics, can be obtained using the low-frequency (24–270 kHz) resonant torsional-oscillation technique [70, 71]. The high accuracy of this method (1–2%) is due to the relative simplicity of the measurement of changes in the resonant frequency Δf and in the half-width δf of the resonance curve of the quartz element as it is immersed in a test medium. The measured resonator characteristics are related in a simple manner to the impedance of the medium:

$$Z = R + iX = K^{-1}(\delta f + i\Delta f), \qquad (5.3)$$

where K is the quartz generator constant. The components of the complex shear modulus $G = G' + i\omega\eta$ are linked to the impedance components by the relations

$$G' = \frac{R^2-X^2}{\rho}, \quad \eta = \frac{RX}{\pi f\rho}. \qquad (5.4)$$

Refs [70, 71] describe a measuring element that eliminates the damping effect of fastening on the resonator finesse and the shunting of the resonator electrodes by a conducting liquid and its vapors (Fig. 11). Four cross-linked electrodes deposited on the cylindrical quartz surface induce torsional oscillations of the resonator. When the electrode-free part of the resonator is submerged in the test medium, the liquid adheres to its end and lateral surfaces, increasing the moment of inertia of the resonator and changing the resonant frequency by a quantity Δf. The range of the measured viscosity coefficients can be extended using a regime of freely dying oscillations of the resonator loaded with the liquid

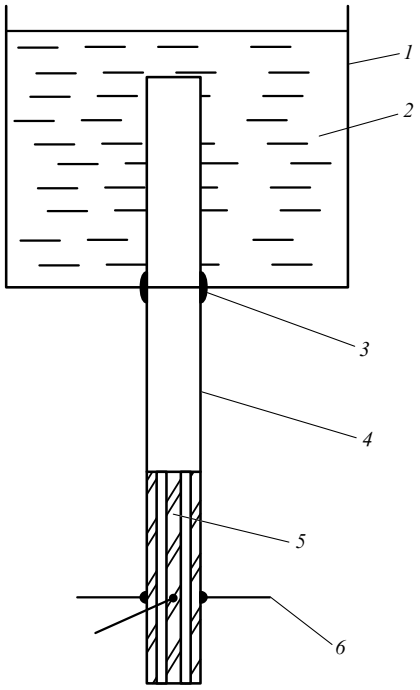

Figure 11. Schematic representation of a measuring element for experiments with the use of the low-frequency resonant torsion oscillation technique [70, 71]: *1*, glass container; *2*, test medium; *3*, glue; *4*, fused quartz cylindrical surface; *5*, quartz crystal; *6*, electrodes.

under study (at η values of up to 2×10^2 Pa s [70, 72]) or with a resonator having an internal cylindrical cavity. It is demonstrated in [70] that a 60 mm high sensor (20 and 10 mm outer and inner diameter, respectively), with a 30 mm deep inner cavity, can be used to measure the viscosity of a liquid until it undergoes vitrification.

The liquid volume may be as small as $0.1-0.5\,\mathrm{cm}^3$, and the size of the resonator unit can substantially reduced if a thin quartz plate is used as the resonator of shear oscillations (Fig. 12) [70, 73]. Gold electrodes, 6 mm in diameter (D2), are placed in the center of a polished quartz plate of thickness $L = 0.34$ mm and diameter $D_1 = 2.5$ mm. In such a construction, the electrodes are located far from the plate edges, so as to confine the oscillation energy beneath the electrodes and avoid the effect of fastening on the resonator finesse. The

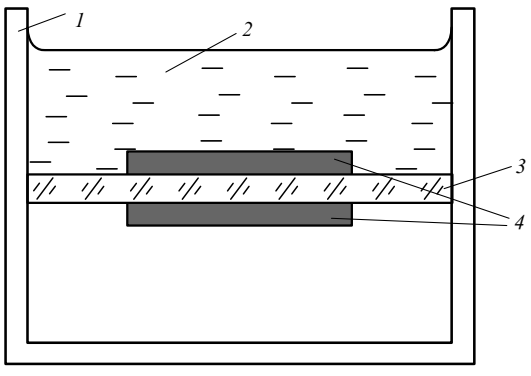

Figure 12. Schematic of the measuring element used in the high-frequency resonance method: *1*, container; *2*, test liquid; *3*, quartz resonator; *4*, electrodes [70].

lower edge of the resonator is insulated from the outer air. The choice of harmonics from the first to the seventh allows the frequency range from 4.9 to 33.9 MHz to be covered. A planar orientation of the NLC at the resonator surface is achieved if a coating of phenyltrichlorosilane is rubbed parallel and perpendicular to the direction of oscillations after the plate is immersed in a 5% solution in toluene and then dried. The homeotropic orientation is secured by treating the surface of the resonator with a 5% dimethyldichlorosilane solution in toluene and subsequently drying. It is shown in [74] that the form of temperature dependences of the active R and reactive X components of the shear acoustic impedance for various NLC orientations relative to the direction of oscillations corresponds to the form of analogous dependences for the three principal NLC viscosities (see Fig. 2). Moreover, the coefficients of viscosity for the three different geometries are virtually frequency-independent. In this case, $\eta_B \neq \eta_C$. In other words, the Rapini relation is not fulfilled, probably because the relaxation times of orientational and translational molecular motions are different [see, for instance, (4.23)]. The failure of the Rapini equality does not mean that the Parodi relation is violated.

The viscosity coefficients η_A and η_B can be obtained by measuring the spectra of inelastic light scattering by capillary waves generated on the free nematic surface [75]. An LC sample of large thickness and diameter (5 and 25 mm, respectively) is placed in a horizontal magnetic field $H \sim 2$ kOe. A laser beam is reflected from the LC free surface and partly scattered at angles controlled the length of thermally induced capillary waves. Wave motion leads to a Doppler shift in the incident light frequency. Both the frequency and damping coefficient depend on the NLC surface tension σ and viscosity η and can be measured spectroscopically. Exact expressions for the spectral energy density of the scattered light are presented in [76, 77]. At low viscosities, the spectrum is Lorentzian, centered at the frequency

$$\nu_q = (2\pi)^{-1}(\sigma q^3)^{1/2}\,, \tag{5.5}$$

with the half width

$$\Delta\nu_\perp = \frac{\eta_A q^2}{\pi\rho} \quad \text{for} \quad q \perp H\,,$$

$$\Delta\nu_{||} = \frac{(\eta_B + \eta_D/8)q^2}{\pi\rho} \quad \text{for} \quad q||H\,, \tag{5.6}$$

where σ is the surface tension; ρ is the NLC density; q is the wave vector showing the direction in which capillary waves propagate, either normal or parallel to the magnetic field; and $\eta_D = \alpha_1 + \gamma_2^2/\gamma_1$. A mathematical processing of the spectrum shape for $q||H$ can yield η_B and η_D separately.

6. Rotating magnetic field method

V N Tsvetkov was the first to report, in 1939 , an experiment in which a liquid crystal was placed in a rotating magnetic field [78, 79]. After the researchers' interest in LCs quickened in the late 1960s and early 1970s, this experiment was applied, almost unmodified, to measuring the rotational viscosity γ_1 [80–83]. Some investigators chose to rotate the sample suspended between the magnet's poles rather than the magnet itself [84]. The geometrical arrangement of this experiment is schematically shown in Fig. 13. If the presence

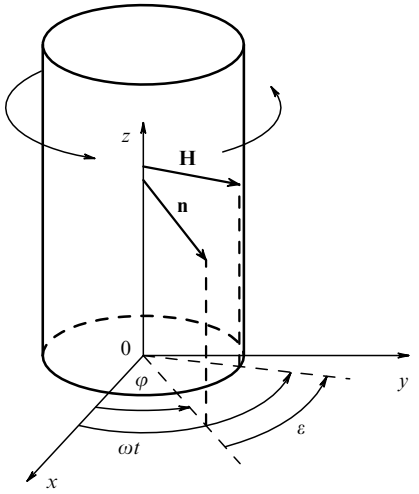

Figure 13. Experimental geometry featuring the relative orientation of the magnetic field vector **H** (phase ωt) and director **n** (phase φ) in the measurement of the rotational viscosity coefficient γ_1 by the rotating field method. The angle ε characterizes the lag of the director behind the magnetic field in a synchronous regime.

of a constant magnetic field **H**, the absence of streams, and uniform orientation are taken into account, the equation of director motion (2.18) has the form

$$\ddot{\varphi} - \gamma_1 \dot{\varphi} + 0.5\rho\chi_a H^2 \sin 2(\varphi - \varphi_H) = 0\,, \tag{6.1}$$

where φ and φ_H are the angles of rotation of the director and magnetic field, respectively.

Let us consider the establishment and relaxation of the director orientation at the beginning and end of magnetic field rotation, and also in the case of small oscillations in the field direction [85]. Under the assumption that the difference $\varphi - \varphi_H$ is small, upon reducing Eqn (6.1) to a linear form, its solution can be written as

$$\varphi = \varphi_0 + \omega_0 t + \int_0^t f(t')\psi_n(t - t')\,\mathrm{d}t'\,, \tag{6.2}$$

where $\varphi_0 = \varphi(t = 0)$ and $\omega_0 = \dot{\varphi}(t = 0)$ are the initial conditions, $n = -1$, 0 and $+1$, and $f(t)$ and $\psi_n(t)$ are given by the expressions

$$f(t) = -\frac{2I\chi_a H^2}{\gamma_1}\left[\varphi_H(t) - \varphi_0 - \omega t\right] - 2\omega_0\,,$$

$$\psi_n(t) = \left[\frac{\sinh(\alpha t/\tau)}{\alpha} + n\cosh\frac{\alpha t}{\tau}\right]\exp\left(-\frac{t}{\tau}\right). \tag{6.3}$$

Here, I is the moment of inertia of unit volume, α is the dimensionless constant related to the critical field strength $H_{cr} = -\gamma_1/(4I\rho\chi_a)^{1/2}$ via the expression $\alpha = (1 - H^2/H_{cr}^2)^{1/2}$, and $\tau = -2I/\gamma_1$ is the damping time. The measurement of the rotational viscosity coefficient by the rotating magnetic field method usually gives the torque density Γ exerted on the wire from a sample unit volume. The quantity Γ is related to the rotational velocity by the simple equation

$$\Gamma = -\gamma_1 \dot{\varphi}\,. \tag{6.4}$$

The insertion of (6.2) into (6.4) with (6.3) taken into account leads to

$$\Gamma = -2\rho\chi_a H^2\left[\varphi_0\psi_0(t) + \frac{1}{\tau}\int_0^t \varphi_H(t')\psi_{-1}(t - t')\,\mathrm{d}t\right] + \gamma_1\omega_0\psi_{+1}(t)\,. \tag{6.5}$$

If a magnetic field with a constant rotation rate ω is applied at the initial time, when $\varphi_0 = 0$ and $\omega_0 = 0$, then $\varphi_H = \omega t$ and the wire is subject to the torque

$$\Gamma = -\gamma_1\omega\left[1 - \psi_1(t)\right]. \tag{6.6}$$

Uniform director rotation sets in within a sufficiently long time.

The inertial terms in (6.1) influence only the time needed for the uniform director orientation to be established. Therefore, at angular velocities below the critical velocity ω_{cr},

$$\omega \leqslant \omega_{cr} = \frac{\chi_a H^2}{2\gamma_1}\,, \tag{6.7}$$

expression (6.2) has a very simple form

$$\varphi = \omega t - \varepsilon\,, \quad \sin 2\varepsilon = \frac{\omega}{\omega_{cr}}\,. \tag{6.8}$$

For $\omega < \omega_{cr}$, the director lags behind the field by a constant angle, and the measurement of γ_1 reduces to finding ε. For $\omega > \omega_{cr}$, Eqn (6.1) admits a solution of the form [84]

$$\tan\left(\varepsilon - \frac{\pi}{4}\right) = \left(\frac{\omega - \omega_{cr}}{\omega + \omega_{cr}}\right)^{1/2}\tan\left[(\omega^2 - \omega_{cr}^2)^{1/2}t - t_0\right], \tag{6.9}$$

where

$$t_0 = \arctan\left(\frac{\omega - \omega_{cr}}{\omega + \omega_{cr}}\right)^{1/2}. \tag{6.10}$$

Therefore, the director rotates with the angular velocity

$$\Omega = (\omega^2 - \omega_{cr}^2)^{1/2}\,. \tag{6.11}$$

If an LC sample of volume V is suspended by an elastic wire, the elastic torque exerted on the sample is

$$M = \Gamma V = \gamma_1\omega V \quad \text{for} \quad \omega < \omega_{cr}\,, \tag{6.12}$$

$$M = 0.5V\chi_a H \quad \text{for} \quad \omega = \omega_{cr}\,, \tag{6.13}$$

$$M = \frac{\gamma_1 V\omega_{cr}^2}{\omega + (\omega^2 - \omega_{cr}^2)^{1/2}} \quad \text{for} \quad \omega > \omega_{cr}\,. \tag{6.14}$$

Figure 14 shows the torque acting on a para-azoxyanisole (PAA) sample at different temperatures plotted against the angular rotation rate of the magnetic field [78]. This dependence was found by V N Tsvetkov in 1939 and confirms the validity of relations (6.12)–(6.14). The left branches of the curves ($\omega < \omega_{cr}$) are in quantitative agreement with the theoretical predictions [formula (6.12)]. For the right branches, the observed M values are slightly higher than the theoretical ones. The best fit of the theory to experimental data for the right branch of the dependence $M(\omega)$ was achieved in [82] where the torque was measured using a hard

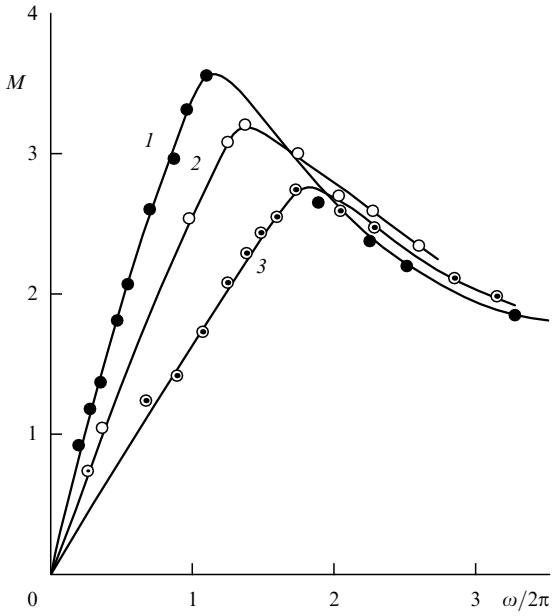

Figure 14. Torque M acting on a PAA sample versus the angular rotation rate of the magnetic field ω at temperatures 12 ° (*1*), 116 ° (*2*), and 120 ° (*3*) [78].

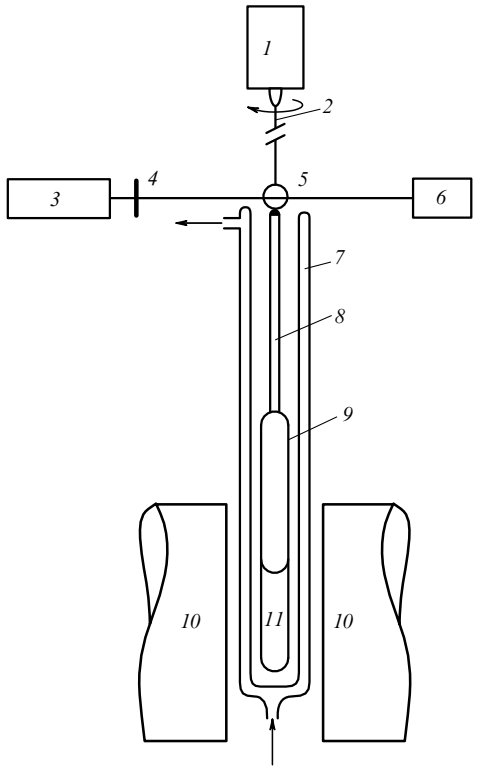

Figure 15. Experimental setup for measuring the viscosity coefficient γ_1 by the rotating magnetic field method [84].

teflon cylinder (used instead of a metal wire) submerged in the liquid sample.

It was shown in [86] that an increase in the magnetic field rotation rate leads to a change in the sample structure. The initial fall of the intensity of satellite lines in the NMR spectrum ends in their complete disappearance for $\omega \gg \omega_{cr}$.

The inertial terms can be found from the relaxation time of torque Γ measured after the magnetic field stops rotating or in an oscillating magnetic field [85]. In the former case, $\varphi_H = 0$, $\varphi_0 = \gamma_1\omega/\rho\chi_a H^2$, and expression (6.5) assumes the form

$$\Gamma = -\gamma_1\omega\psi_1(t)\,. \tag{6.15}$$

The torque Γ decreases monotonically for $H \leqslant H_{cr}$ and in the process of damped oscillations for $H > H_{cr}$.

Now, we describe in brief the experimental setup and discuss potential measuring errors intrinsic in the rotating magnetic field method. Figure 15 is a diagrammatic representation of the apparatus used in [84]. The sample tube *9* (5 or 30 mm in diameter) is filled with the liquid crystal *11* to a height of about 80 mm (such a height is needed to avoid bottom effects) and is suspended on the glass bar *8* and the torsion wire *2* (iron wire, 1 m in length and 30 or 100 μm in diameter). The tube and the liquid can be rotated by the stepping motor *1* (500 steps per revolution). The sample is placed between the poles *10* of an electromagnet (200 mm core diameter, 50 mm pole gap, $B = 0$ to 1.3 T) and surrounded by a double-walled glass tube *7* which is kept at constant temperature by a water thermostat. The rotational viscosity coefficient can be determined from the torsion angle of the wire as

$$\gamma_1 = \frac{D\alpha}{\dot{\theta}V}\,, \tag{6.16}$$

where D is the torsion constant of the wire and $\dot{\theta}$ is the angular velocity of the stepping motor. The torsion angle α can be found from the phase lag between the stepping motor and the sample tube that arises after switching-on the magnetic field. The laser *3*, cylindrical lens *4*, mirror *5*, and six photodiodes *6* mounted 60° apart in a horizontal plane, form the detection system for the phase lag. The differences between the phase lags with and without the magnetic field are averaged by a computer over several revolutions. Deviations from the Hooke law at large torsion angles of the wire are taken into account as well as the residual torsion (which persists as long as the magnetic field is applied due to the viscosity of the air between the sample and the thermostated tube) and errors arising from the noncoaxial position of the sample.

These uncertainties are small compared to the serious errors that can result from wall effects, such as the backflow, inversion walls, and elastic torques attributable to incomplete orientation of the LC by the magnetic field. Indeed, an LC flow opposite in sign to that of the magnetic field rotation is known to occur near the tube wall. However, this flow should not be identified with the normal backflow [19, 20] created by differently directed streams. Most likely, it is produced by the backflow between the cylinder wall and the free surface in the upper part of the sample. The velocity of this flow is higher than that of the direct one. The theory of a similar effect was proposed in [21]. Under the boundary condition $v = 0$ at the cylinder wall, elastic forces preclude the complete orientation of the sample by the magnetic field at distances of the order of the magnetic coherence length [87]

$$\xi = \pi H^{-1}\left(\frac{K_{ii}}{\chi_a}\right)^{1/2}. \tag{6.17}$$

This accounts for the smaller effective radius of the rotating LC sample and, accordingly, the smaller torque of the wire.

The effective value of the measured rotational viscosity coefficient is [84]

$$\gamma_1^{\text{eff}} = \gamma_1\left(1 - \frac{2\xi}{R}\right). \tag{6.18}$$

An even greater influence on γ_1 is exerted by the inversion walls (resembling the well-known Bloch walls in ferromagnetic materials), which separate the LC sample into domains with different director orientations [88, 89]. Both the stability and topology of such walls are considered in [84, 89]. Their relaxation time can be obtained from the balance of the viscous, magnetic, and elastic energies as

$$\tau \cong \frac{\pi\gamma_1}{\chi_a B^2}, \tag{6.19}$$

which gives about 0.1 s for methoxybenzylidene butylaniline (MBBA) at room temperatures and $B = 1$ T. Since this relaxation time is comparable with the revolution time of the sample in the magnetic field, this mechanism should substantially affect the quantity γ_1^{eff}.

The part of the sample occupied by the inversion walls, does not appreciably contribute to the torque M and can be taken into account, to a first approximation, by replacing ξ with the larger quantity $\xi^* = c\xi$ in expression (6.18). Calculations show that to $\xi^* = 9\xi$ for two inversion walls. The effect of the walls or, in their absence, the influence of the elastic forces on the measurements can be reduced by using stronger magnetic fields and/or sample tubes of larger diameters. With the rotating magnetic field method, the authors of [84] managed to measure γ_1 to an accuracy of 0.3% or so. However, this requires a large amount of substance ($\sim$ 70 g). was needed to achieve such a high accuracy. For this reason, many investigators who use smaller samples to measure γ_1 [82, 83], report lower values than those obtained with the same method or other methods described in Sections 7 and 8.

The phase lag between the directions of the magnetic field and director (and hence, the γ_1 value) can be found by examining the EPR spectrum of a paramagnetic label dissolved in the NLC rotating in a magnetic field [86] and also by acoustic methods measuring the anisotropy of the ultrasound velocity [90–91] or the anisotropy of the ultrasound absorption coefficient [92, 93]. In the last two cases, it is possible to measure the anisotropy of diamagnetic susceptibility at a known rotational viscosity.

Ultrasonic methods are convenient when the torque or the optical parameters of the NLC cannot be directly measured, e.g. in experiments with samples under high pressure [94].

Since the intermolecular distance decreases with increasing pressure, measurements of the nematic viscosity under varying external pressure make it possible to establish the relationship between viscosity, on the one hand, and molecular packaging and free volume, on the other hand. For this reason, the measurement of the NLC viscosity as a function of pressure is important in itself. The dynamic viscosity was measured in [67] by a falling ball technique and the rotational viscosity, in [94] by a rotating magnetic field method. In general, the construction of the cell for measuring the rotational viscosity under high pressure and the signal recording technique described in [94] are similar to those reported in [84] (see Fig.15). In the experiment, the wire is initially rotated in such a way that the plane of the mirror be perpendicular to the light beam. The magnet is rotated so as to make the director rotation angle equal to 180°. Thereafter, these operations are repeated in an inverse order. In view of (6.12) and (6.16),

$$\gamma_1 = \frac{(\varphi_{\text{rig}} - \varphi_{\text{lef}})D}{(\omega_{\text{rig}} - \omega_{\text{lef}})V} = \frac{2\pi D}{(\omega_{\text{rig}} - \omega_{\text{lef}})V}, \tag{6.20}$$

where ω_{rig} and ω_{lef} are the right and left rotation rates of the magnet, respectively.

It is difficult to measure the torque to a high accuracy; however, the quantity γ_1 can be determined by measuring the ultrasound absorption anisotropy $\varepsilon = \Delta\alpha/f^2$ in a pulsed or rotating magnetic field [95–99], and also in a static magnetic field ($\omega = 0$) [100–103]. In the former case, the time-dependent response of $\Delta\alpha/f^2$ is described by the expression [95]

$$\Delta\alpha(t) = \alpha_{||}(t) - \alpha(0) = c\left[\langle\cos^2\theta(t)\rangle - \frac{1}{3}\right] + b\left[\langle\cos^4\theta(t)\rangle - \frac{1}{5}\right], \tag{6.21}$$

where the relationship between the director displacement angle $\theta(t)$ and the magnetic field growth time in an electromagnet, τ_H, a function of the inductivity of the magnet ($H(t) = H_{\max}[1 - \exp(-t/\tau_H)]$), is described by the following functional relations:

$$\langle\cos^2\theta(t)\rangle = \frac{1 - \left[A/(1-A)\right]^{1/2}\arccos A^{1/2}}{1 - A},$$

$$\langle\cos^4\theta(t)\rangle = \frac{1 + A/2 - (3/2)\left[A/(1-A)\right]^{1/2}\arccos A^{1/2}}{(1-A)^2},$$

$$A = \exp\left\{-\frac{\chi_a H^2}{\gamma_1}\left[2t - 3\tau_H + 4\tau_H\exp\left(-\frac{t}{\tau_H}\right) - \tau_H\exp\left(-\frac{2t}{\tau_H}\right)\right]\right\},$$

where c and b are coefficients characterizing the dependence of ultrasound absorption anisotropy on the angle β between the wave vector and the director:

$$\alpha(\beta) = \alpha_0 + c\cos^2\beta + b\cos^4\beta \tag{6.22}$$

or, if we neglect the small contributions of thermal conductivity and capacity [10],

$$\alpha(\beta) = \frac{\omega^2}{2\rho C_0}\left[(\nu_2 + \nu_4) + 2(-\nu_2 + 2\nu_3 - \nu_4 + \nu_5)\cos^2\beta + 2(\nu_1 + \nu_2 - 2\nu_3)\cos^4\beta\right], \tag{6.23}$$

where ν_i is the Forster coefficient of viscosity, ρ is the NLC density, and C_0 is the ultrasound speed. It follows from the medium incompressibility condition that $\nu_2 = \nu_4$, $\nu_5 = 0$. In routine acoustic measurements ($f = 620$ MHz, as in [104, 105]), a nematic can be regarded as a quasi-incompressible medium. Then, the coefficients ν_1, ν_2, and ν_3 can be obtained directly from high-frequency measurements of the ultrasound absorption coefficients [105]

$$\nu_1 = \left(\frac{\alpha^{||}}{f^2}\right)_{620}\frac{\rho C_0^3}{4\pi^2}, \quad \nu_2 = \left(\frac{\alpha^{\perp}}{f^2}\right)_{620}\frac{\rho C_0^3}{4\pi^2},$$

$$2\nu_3 = \nu_1 + \nu_2 = \frac{\Delta\alpha}{f^2}\,\frac{\rho C_0^3}{4\pi^2}. \tag{6.24}$$

The characteristic time of disorientation after switching-of the magnetic field can be estimated from the intensity of the saturation field $H_{\rm sat}$:

$$\tau_{\rm cr} = \frac{\gamma_1}{\chi_{\rm a} H_{\rm sat}^2} \,. \tag{6.25}$$

In a rotating magnetic field, the phase shift of the director rotation in a synchronous regime ($\omega_H < \omega_{\rm cr}$) under the condition $\varphi(t=0)=0$, measured by ultrasonic methods, is described by the expression [96]

$$\varphi = \arctan \frac{1-\exp\left[-2\omega_H t(\varepsilon^2-1)^{1/2}\right]}{\left[\varepsilon+(\varepsilon^2-1)^{1/2}\right]-\left[\varepsilon-(\varepsilon^2-1)^{1/2}\right]\exp\left[-2\omega_H t(\varepsilon^2-1)^{1/2}\right]} \,, \tag{6.26}$$

where $\varepsilon = \chi_{\rm a} H^2/2\gamma_1\omega_H$. Expressions for ultrasound absorption anisotropy in an asynchronous regime ($\omega > \omega_{\rm cr}$) are given in [96]. It follows from (6.21) and (6.26) that ultrasonic methods for recording the director rotation measure the ratio $\gamma_1/\chi_{\rm a}$. Therefore, to determine γ_1, it is necessary to know the diamagnetic anisotropy $\chi_{\rm a}$, which is more difficult to measure than the NLC density. The volume of the working chamber is 5.3 cm^3, which, for a given ultrasound frequency (2.8 MHz) and pulse duration, makes it possible to reduce the errors related to the pulse spectrum length and the broadening and interference of the incident and reflected beams.

NMR spectroscopy is frequently used to measure some parameters at weak magnetic field oscillations about a certain average direction. In this case, $\varphi_H = \sigma\exp(i\kappa t)$, where $\sigma \ll 1$. The substitution of this φ_H into (6.5) with taking into account the initial conditions $\varphi_0 = 0$, $\omega_0 = 0$ for the torque gives

$$\Gamma = \rho\chi_{\rm a} H^2 \sigma \left[-\frac{2}{\tau_0}\int_0^t \exp(\mathrm{i}\kappa x)\psi_{-1}(x)\,\mathrm{d}x \right] . \tag{6.27}$$

Within a sufficiently long time, oscillations establish in the torque Γ. They lag behind the magnetic field direction by the angle $\theta \pm \pi$:

$$\Gamma = \rho\chi_{\rm a} H^2 \sigma \cos\theta \exp\left[\mathrm{i}(\kappa t - \theta)\right] . \tag{6.28}$$

The angle θ is determined as

$$\tan\theta = \frac{\rho\chi_{\rm a} H^2}{\gamma_1 \kappa}\left[1 - \left(\frac{\kappa}{\kappa_{\rm cr}}\right)^2\right] . \tag{6.29}$$

Evidently, at $\kappa = \kappa_{\rm cr} = (\rho\chi_{\rm a} H^2/I)^{1/2} = H/H_{\rm cr}\tau$, the torque Γ changes in synchrony with the direction of the magnetic field H. For this reason, $\kappa_{\rm cr}$ is termed the angular velocity of synchronization. Knowing the torque amplitude and phase lag, makes it possible to determine the density of the moment of inertia I.

Gerber [106] described a capacitance method for recording the dynamics of the director reorientation due to small changes in the direction of the magnetic field. A measuring capacitor filled with the LC is placed between the pole caps of a magnet generating fields H of up to 8 kOe. A pair of coils mounted in the pole gap generate a weak reorienting magnetic field H_1 of about 10 Oe. The normal to the capacitor plates makes angles of 45° with respect to the mutually perpendicular directions of $\mathbf{H}$ and $\mathbf{H}_1$. The strength H and the capacitor gap thickness are chosen so as do minimize the magnetic coherence length (6.17). The field H_1 of the coils, controlled through a squared-pulse wave generator, is suddenly reversed, thus rotating the total field $\mathbf{H}+\mathbf{H}_1$ by several milliradians. The resulting change in the director orientation leads to a change in the sample capacitance C:

$$\frac{1}{C}\,\frac{\mathrm{d}C}{\mathrm{d}\theta} = \frac{2(\varepsilon-\varepsilon_\perp)}{\varepsilon+\varepsilon_\perp} \,. \tag{6.30}$$

The relaxation time of the measured capacitance change is

$$\tau = \frac{\gamma_1}{\chi_{\rm a} H^2} \,. \tag{6.31}$$

The error of measuring γ_1 by this method is of the order of 6%, depending on the accuracy of the recording procedure and the determination of $\chi_{\rm a}$ from the variation in the threshold voltage $U_{\rm F}$ for the Freedericksz transition in the magnetic field [107], and on the approximation of the temperature dependence $\chi_{\rm a}$ by the temperature dependence of birefringence Δn.

7. Methods based on studying LC reorientation in magnetic and electric fields

If an LC layer between two substrate plates is subject to an external magnetic or electric field, it undergoes deformation characterized by director reorientation. This effect depends on the boundary conditions at the substrates and on the magnitude and sign of the diamagnetic or dielectric permittivity. It is named for V K Freedericksz, who was the first to observe it [108]. A detailed description of the Freedericksz transition can be found in [1, 109]. Three particular cases differing in director and external field orientations with respect to the substrate plates are of practical importance and can easily be observed in experiments (Fig. 16). Deformations induced by a magnetic or electric field whose strengths exceeds a certain critical (threshold) value $H_{\rm F}$ or $E_{\rm F} = U_{\rm F}/L$ (L is the layer thickness), respectively, are referred to as splay, twist, and bend elastic deformations or, following the notation adopted in [1], S-, T-, and B-effects. The threshold values $H_{\rm F}$ and $U_{\rm F}$ are given by the relations

$$H_{\rm F} = \frac{\pi}{L}\left(\frac{K_{ii}}{\chi_{\rm a}}\right)^{1/2}, \quad U_{\rm F} = 2\pi\left(\frac{\pi K_{ii}}{\varepsilon_{\rm a}}\right)^{1/2}, \tag{7.1}$$

where $\chi_{\rm a}$ and $\varepsilon_{\rm a}$ stand for the anisotropies of diamagnetic and dielectric permittivity, respectively, and K_{ii} for the Frank elastic moduli: $K_{ii} = K_{11}$ for the S-effect, $K_{ii} = K_{22}$ for the T-effect, and $K_{ii} = K_{33}$ for the B-effect. In dynamic studies of the Freedericksz transition, it is possible to measure the coefficient of rotational viscosity γ_1. In this case, the viscoelastic relation is usually determined for the NLC. In addition, the corresponding coefficient of elasticity is needed

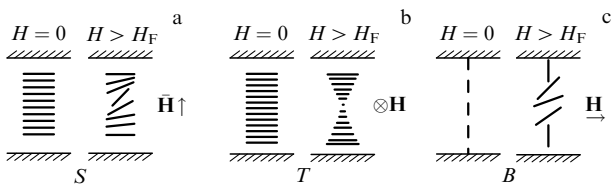

Figure 16. Director and field orientations for the S-, T-, and B-effects induced by an electric or magnetic field.

and can be measured using the same sample. The main equations of director reorientation in an NLC layer for the above three deformations are presented in [110].

The progressive motion of molecular centers of gravity is absent only in the case of torsional strain, where the equation of motion has the simplest form [35]:

$$K_{22}\frac{\partial^2\varphi}{\partial z^2}+\chi_a H^2\sin^2\varphi\cos\varphi=\gamma_1\frac{\partial\varphi}{\partial t}\,, \tag{7.2}$$

where φ is the director torsion angle. For a field slightly stronger than the threshold one, H_F, φ is small and the solution satisfying the boundary conditions $\varphi(z=\pm L/2)=0$ has the form

$$\varphi=\varphi_{\max}\cos\frac{\pi z}{L}\,. \tag{7.3}$$

Expression (7.3) holds for values below $\varphi_{\max}\approx 40^\circ$ [111]. After the field H is switched off, the deformation relaxes according to the exponential law

$$\varphi(z,t)=\varphi(z,0)\exp\left(-\frac{t}{\tau_0}\right), \tag{7.4}$$

where the relaxation time τ_0 is given by the expression

$$\tau_0=\frac{\gamma_1 L^2}{\pi^2 K_{22}}\,, \tag{7.5}$$

and $\varphi(z,0)$ by expression (7.3).

The variation of $\varphi(z,t)$ is traced by the rotation of the conoscopic figure observable with a polarizing microscope in a planar oriented LC layer subject to a magnetic field **H** parallel to the layer plane and perpendicular to the director **n** (Fig. 16b) [111, 112]. In the case of torsional strain, the conoscopic figure turns through an angle δ given by the following expression [112]:

$$\tan 2\delta=\frac{\langle\sin 2\varphi(z)\rangle}{\langle\cos 2\varphi(z)\rangle}=\frac{2\sin\varphi}{\left[2E(1/2\pi,\sin\varphi_{\max})-F(1/2\pi,\sin\varphi_{\max})\right]}\,, \tag{7.6}$$

where F and E are the complete elliptical integrals of the first and the second kind, respectively. However, at $\mathbf{H}\perp\mathbf{n}$, the conoscopic figure can rotate both clockwise and counterclockwise. This situation takes place in experiment and precludes accurate measurements [113]. The problem can be resolved by aligning **H** at an angle of $90-\varphi_0$ with respect to **n**. This results in a more complicated form for expression (7.6) [91]:

$$\tan 2\delta=\frac{2(\sin^2\varphi_{\max}-\sin^2\varphi_0)^{1/2}\cos 2\varphi_0-H(\psi_0,\varphi_{\max})\sin 2\varphi_0}{2(\sin^2\varphi_{\max}-\sin^2\varphi_0)^{1/2}\sin 2\varphi_0-H(\psi_0,\varphi_{\max})\cos 2\varphi_0}\,,$$

$$\sin\psi_0=\sin\varphi_0\sin\varphi_{\max}\,, \tag{7.7}$$

$$H(\psi_0,\varphi_{\max})=2\int_{\psi_0}^{\pi/2}d\psi(1-\sin^2\varphi_{\max}\sin^2\psi)^{1/2}\times\int_0^{\pi/2}d\psi(1-\sin^2\varphi_{\max}\sin^2\psi)\,.$$

The angle δ shows a linear dependence on $\varphi_{\max}$ until $\varphi_{\max}\approx 40^\circ$ [111]. A typical dependence of δ on time t is shown in Fig. 17a. It can be used to calculate γ_1 if the elastic constant K_{22} is known.

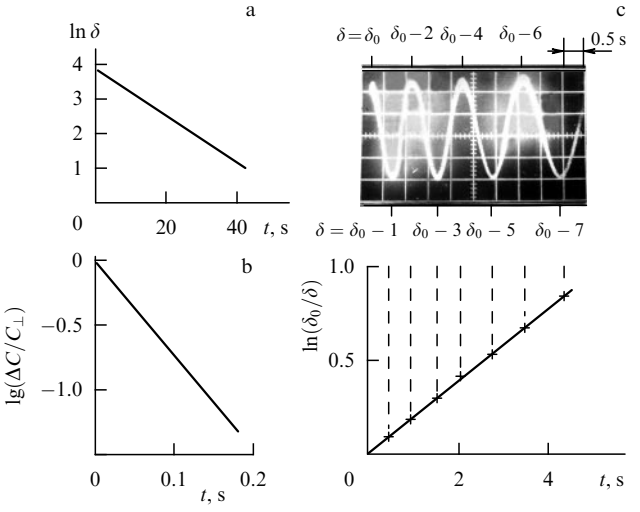

Figure 17. Relaxation of the rotation angle of the conoscopic figure for (a) *T*-deformation [111], (b) reduced capacitance $\Delta C/C_\perp$ [106], and (c) phase lag *S*-deformation [115] and light transmission by crossed polaroids.

For *S*- and *B*-effects, the situation is somewhat more complicated because of the backflow due to director reorientation [19]; in this case, instead of measuring the coefficient of rotational viscosity γ_1, its effective value γ_1^{eff} is actually obtained. The associated corrections for γ_1^{eff} are different for the initially planar and homeotropic orientations because of the difference in the torque exerted on an elementary NLC volume [20]. For the *S*-effect,

$$\gamma_1^{\text{eff}}=\eta_S=\gamma_1-\frac{\alpha_3^2}{\eta_1}\approx\gamma_1\,. \tag{7.8}$$

For the *B*-effect,

$$\gamma_1^{\text{eff}}=\eta_B=\gamma_1-\frac{\alpha_2^2}{\eta_2}\,. \tag{7.9}$$

A comparison of these expressions shows that the measurement of the rotational viscosity coefficient in the case of splay deformation (Fig. 16a) entails a small error (of less then 1%), since $\alpha_3\ll\gamma_1,\eta_S$ [16, 24]. As a rule, this error is smaller than that introduced by laboratory instruments or data processing procedures. In the case of bend deformation (Fig. 16c), the correction not only substantially reduces the measured γ_1, but also strongly affects its temperature dependence. For this reason, when γ_1 is determined from the relaxation of *SB*-deformation, an originally planar orientation is usually chosen and the director tilt angle is found from the change of the phase lag $\Delta\Phi$ [114] or capacitance [115] of the NLC layer. In either case, the deformation of the LC layer is induced by an external electric field. The equation of director relaxation after the field is removed acquires the form [114]

$$\gamma_1^{\text{eff}}\frac{\partial\theta}{\partial t}=(K_{11}\cos^2\theta+K_{33}\sin^2\theta)\frac{\partial^2\theta}{\partial z^2}+(K_{33}-K_{11})\sin\theta\cos\theta\left(\frac{\partial\theta}{\partial z}\right)^2. \tag{7.10}$$

For small deformations, $\theta \ll 1$; therefore, in view of (7.8), expression (7.10) can be written in the simpler form

$$\eta_S \frac{\partial\theta}{\partial t} = K_{11} \frac{\partial^2\theta}{\partial z^2} . \tag{7.11}$$

It admits an exponential solution for θ, similar to (7.4), with the time constant

$$\tau_0 = \frac{L^2}{\pi^2} \frac{\eta_S}{K_{11}} . \tag{7.12}$$

In an optical study of splay (or bend) elastic deformation, a change in the director tilt angle θ leads to a change in the effective birefringence of the NLC layer and, therefore, to a change in the phase lag $\Delta\Phi$, which manifests itself in an oscillatory transmittance of the cell placed between crossed polaroids, depending on the voltage applied or on time, if the voltage is switched off. A change in transmittance from minimum to maximum or vice versa corresponds to a change in $\Delta\Phi$ by π radians. If the phase lag changes by δ_0 radians after a voltage $U > U_F$ is switched on, then recording the time points of transmittance extrema after the voltage is removed gives the time dependence of the phase lag change $\delta = \Delta\Phi_{max} - \Delta\Phi$ with respect to the lag for the undistorted layer (Fig. 17c). The phase lag relaxation curve is described by the equation

$$\ln\left(\frac{\delta_0}{\delta}\right) = \frac{2\pi^2}{L^2} \frac{K_{11}}{\gamma_1} t , \tag{7.13}$$

i.e. the relaxation time of the director tilt angle is twice as long as that of the phase lag δ. The approximations described by Eqns (7.11), (7.13) do not work for increased NLC deformations.

This method for the measurement of the relaxation time allows the change in the viscoelastic ratio η_B/K_{33} to be estimated as a function of the pressure p [116, 117], using a specially designed cell. The elevation of pressure from 10^5 to 5×10^7 Pa leads to a 1.7-fold increase in the viscoelastic ratio (from 2.3 to 3.9 Pa s H^{-1}) due to the decrease of the free volume and the increase of the order parameter. The η_B/K_{33} ratio for MBBA at 35 °C agrees with the values obtained in [117].

An expression analogous to (7.13) can also be derived for the relative change in the capacitance of a planar oriented NLC layer [115]:

$$\frac{\Delta C(t)}{C_\perp} \sim \frac{\varepsilon_a}{2\varepsilon_\perp} \theta_{max} \exp\left(-\frac{2t}{\tau_0}\right) , \tag{7.14}$$

where ε_a is the dielectric anisotropy, $\varepsilon_\perp$ and $C_\perp$ are the dielectric constant and capacitance for the direction perpendicular to the director, θ_{max} is the director tilt angle in the middle of the layer, and $\Delta C = C(t) - C_\perp$ is the change in the layer capacitance following the removal of the voltage. The time dependence of capacitance is shown in Fig. 17b.

Expression (7.14) also describes the change in the nematic twist-cell capacitance in the case of orthogonal director orientations at the opposite substrate plates for $U > U_F$, which implies negligible changes in the azimuthal angle [118].

The viscoelastic ratio $\eta_S/K_{11} \approx \gamma_1/K_{11}$ can be obtained directly from the relaxation time for the electrooptic twist-effect response, T_{off}. For this purpose, the time is measured in which the intensity of the light transmitted by the nematic twist cell sandwiched parallel between two polaroids changes from the maximum (at the time of switching off the applied voltage) to a level of 0.1. Figure 18 plots $\eta_S/K_{11} \approx \gamma_1 K_{11}$ values obtained from the phase lag relaxation time in a planar oriented layer (horizontal axis) versus the switch-off time of electrooptic twist-effect response (vertical axis) for a number of liquid-crystal materials manufactured in Russian and other countries [119, 120]. All points fall, to a high accuracy, on the straight line described by the formula

$$T_{toff} = 0.05 L^2 \frac{\eta_S}{K_{11}} , \tag{7.15}$$

which coincides with the formula describing the relationship between the phase lag relaxation time and the viscoelastic ratio, because $(2\pi^2)^{-1} \approx 0.05$ [see (7.12)].

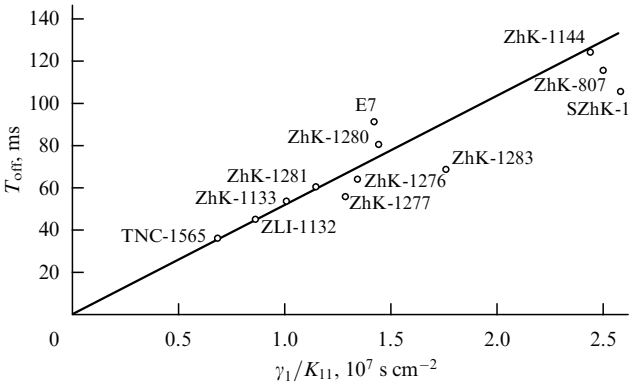

Figure 18. Switch-off times (T_{off}) for the twist-cell optical response as a function of the viscoelastic ratio γ_1/K_{11} for various liquid-crystalline materials. \

The relaxation time of director orientation can be found not only by measuring the capacitance of the LC layer but also by measuring its resistance [121]. To eliminate the effects of near-electrode layers, thick (1 mm) para-azoxyanisole samples were used. The director was planar oriented at the surface of stainless steel gold-plated electrodes. The realignment of the LC layer was accompanied by changes in its resistance from R_t (for the director perpendicular to the field) to R_a (for the director parallel to the field). At an arbitrary voltage, the resistance R was related to the displacement angle φ measured from the normal to the conducting substrate surfaces (z-axis), by the equation

$$R = R_t \int_0^1 (1 + \sigma' \cos^2\varphi)^{-1} \, d\xi , \tag{7.16}$$

where σ' is a constant depending on the NLC elasticity coefficients and $\xi = 2z/L$ is the coordinate normalized to the thickness L (the boundary conditions are $\varphi = 90°$ at $\xi = \pm 1$ and $d\varphi/d\xi = 0$ at $\xi = 0$, i.e. in the center of the cell). At the initial time $t = \tau = 0$ [$t = (L^2\gamma_1/2K_{33})\tau$], the resistance R_0 is described by the average displacement angle φ_0:

$$\frac{R_t - R_0}{R_a - R_0} \frac{R_a}{R_0} = \cos^2\varphi_0 . \tag{7.17}$$

Then, the resistance relaxation upon switching off the electric field is described by the equation

$$\beta_0 = \frac{R - R_0}{R_t - R_0} = \frac{(1 + \sigma' \cos^2\varphi_0) \int_0^1 (1 + \sigma' \cos^2\varphi)^{-1} \, d\xi - 1}{\sigma' \cos^2\varphi_0} . \tag{7.18}$$

The relaxation law for the displacement angle $\varphi(\xi, t)$ can be obtained by means of numerical solution of Eqn (7.10). Upon substituting $\varphi(\xi, t)$ into (7.18), specifying φ_0, and using the reference K_{11}/K_{33} values, β_0 can be calculated and compared with experimental values. The coincidence of these dependences and γ_1 values for para-azoxyanisole [$\gamma_1(121.9\,^\circ\mathrm{C}) = 0.072$ Pa] with the results of other studies confirms the applicability of this approach to the measurement of the coefficients determining the director reorientation rate in NLCs.

It was shown in [122] that, by measuring the current across the cell, it is possible to determine not only the rotational viscosity of an NLC but also the tilt angle of the director at the substrates.

Ref. [19] presents a solution to a (7.12)-type equation that describes the increase and decrease in the deformation of an LC layer at magnetic fields H stronger or weaker than the threshold field H_{cr} (assuming $H/H_{\mathrm{cr}} - 1 \ll 1$). If the displacement angle $\theta(z)$ is small (z is the a coordinate measured perpendicular to the cell plane), it is safe to state that, to a good accuracy,

$$\theta(z, t) = \theta_{\max}(t) \cos \frac{\pi z}{L}\,, \tag{7.19}$$

where $\theta_{\max}$ is the displacement angle of the LC layer. Then, Eqn (7.10) describing the reorientation of the layer reduces to

$$\frac{\gamma_1^{\mathrm{eff}}}{\chi_{\mathrm{a}} H^2} \frac{\mathrm{d}\theta_{\max}}{\mathrm{d}t} = \left[1 - \left(\frac{H_{\mathrm{cr}}}{H}\right)^2\right] \theta_{\max}\,. \tag{7.20}$$

Its solution is

$$\theta_{\max}^2(t) = \frac{\theta^2(\infty)}{1 + [\theta^2(\infty)/\varepsilon^2 - 1] \exp[-(2\chi_{\mathrm{a}} H_{\mathrm{cr}}^2/\gamma_1)(H^2/H_{\mathrm{cr}}^2 - 1)t]}\,, \tag{7.21}$$

where $\theta(\infty) = \theta_{\max}(t \to \infty)$, and $\varepsilon^2 = \langle \theta_{\max}^2(t = 0) \rangle$ reflects the level of orientation fluctuations in the unperturbed state related to the strength of the magnetic field as

$$\varepsilon^2 = \frac{k_{\mathrm{B}} T}{2\pi L K} \ln\left(1 + \frac{H^2/H_{\mathrm{cr}}^2 - 1}{1 - H^2/H_l^2}\right). \tag{7.22}$$

In (7.22), H_l is a certain critical field, which takes into account the finite size of the sample. The fluctuations determine a rise in θ at the beginning of the reorientation:

$$\theta_{\max}^2(t) = \varepsilon^2 \exp \frac{2t}{\tau}\,, \tag{7.23}$$

where τ is the time constant:

$$\tau^{-1}(H) = \frac{\chi_{\mathrm{a}} H_{\mathrm{cr}}^2}{\gamma_1} \left(\frac{H^2}{H_{\mathrm{cr}}^2} - 1\right), \tag{7.24}$$

either a positive or negative at different H/H_{cr} (obviously, $\theta(\infty) = 0$ at $H < H_{\mathrm{cr}}$).

If monochromatic polarized light propagates in an LC layer along the z-axis, the phase difference between the ordinary and the extraordinary beam, depending on the displacement angle $\theta_{\max}(t)$, results in an oscillatory time dependence of the light intensity after the passage of the analyzer. The number $N(t)$ of oscillations is proportional to $\theta_{\max}^2(t) = \theta_{\max}^2(0) \exp(t/\tau)$ (Fig. 17c). The time interval between two neighboring extrema with numbers $N+1$ and N (in the case of a planar orientation of the LC layer, the lower number corresponds to a smaller deformation, i.e. a greater phase lag) is

$$\tau_N = \tau \ln \frac{N+1}{N} \quad \text{at} \quad H > H_{\mathrm{cr}}\,, \tag{7.25}$$

$$\tau_N = \tau \ln \frac{N}{N+1} \quad \text{at} \quad H < H_{\mathrm{cr}}\,. \tag{7.26}$$

In view of (7.25), expressions (7.25) and (7.26) indicate that the quantity $\gamma_1^{\mathrm{eff}}/\chi_{\mathrm{a}}$ or $\gamma_1^{\mathrm{eff}}/K_{ii}$ can be determined from the time interval τ_N. However, the accuracy of the calculation increases if the complete director relaxation process is considered.

Certain tasks require the knowledge of the effective viscosity coefficient for an arbitrary displacement angle of the LC layer. Specifically, such knowledge is necessary when considering a partial NLC reorientation regime realized in matrix-addressed liquid crystal displays or spatio-temporal light modulators. In this case, the reorientation of the NLC does not start from zero angle $\theta = 0$, nor does it end at $\theta = 90^\circ$. Instead, it is determined by the angle given by the applied initial and final bias voltages U and described by an expression derived on the assumption that $K_{11} = K_{33} = K$ and $\varepsilon_{\mathrm{a}} \ll \varepsilon_\perp$ [21]

$$\gamma_1^{\mathrm{eff}} \frac{\partial\theta}{\partial t} = K \frac{\partial^2\theta}{\partial z^2} + \frac{\varepsilon_{\mathrm{a}} E^2}{4\pi} \sin\theta\cos\theta - R(t) \frac{\varphi}{\psi}\,, \tag{7.27}$$

where

$$R(t) = \int_0^L \frac{\varphi}{\psi} \frac{\partial\theta}{\partial t}\,\mathrm{d}z \left(\int_0^L \frac{\mathrm{d}z}{\psi}\right)^{-1}.$$

The effective rotational viscosity γ_1^{eff} is related to the functions that describe the director rotation (φ) and the NLC flow (ψ), i.e. the backflow, by the expressions

$$\begin{aligned} &\eta^{\mathrm{eff}} = \gamma_1^{\mathrm{eff}} = \gamma_1 - \frac{\varphi^2}{\psi}\,, \quad \varphi = \alpha_3 \cos^2\theta - \alpha_2 \sin^2\theta\,, \\ &\psi = \alpha_1 \cos^2\theta \sin^2\theta + 0.5(\alpha_3 + \alpha_6)\cos^2\theta \\ &\quad + 0.5(\alpha_5 - \alpha_2)\sin^2\theta + 0.5\alpha_4\,. \end{aligned} \tag{7.28}$$

The expression for ψ coincides with (3.1) if the azimuthal angle is zero. A study of the partial realignment of planarly and homeotropically oriented NLC layers, which corresponds to a 1π change in the phase delay of the transmitted light [21], has shown that Eqn (7.27) describes experimental findings fairly well. This means that the angular dependence of the effective viscosity can be described by expressions (7.28). It is easy to demonstrate that at $\theta = 0^\circ$ $\gamma_1^{\mathrm{eff}} = \eta_S$ and at $\theta = 90^\circ$ $\gamma_1^{\mathrm{eff}} = \eta_B$. Figure 19 illustrates the dependence $\eta^{\mathrm{eff}}(\theta)$ constructed using the Leslie coefficients α_i reported in [16].

In the foregoing, we have considered spatially uniform director reorientation depending only on the distance from the substrate plates (z-coordinate). Ref. [123] deals with the relaxation of an NLC in which a spatially nonuniform orientation of characteristic size L_{a} is set in one way or another. The correlation length of the order parameter is ξ_0, the characteristic length of variations in the spatially nonuniform orientation is $l_{\mathrm{a}} = (D_{\mathrm{a}}\tau_{\mathrm{a}})^{1/2}$ (where D_{a} is the diffusion

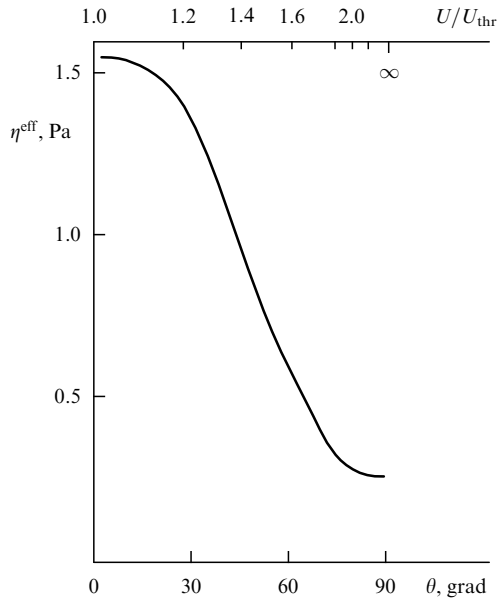

Figure 19. Dependence of the effective NLC rotational viscosity $\eta^{\rm eff}$ on the director alignment angle θ in a planar oriented NLC layer [21]. The upper axis represents the threshold-reduced bias voltage $U/U_{\rm thr}$ corresponding to the director reorientation angle θ in the middle of the NLC layer.

coefficient), and $\tau_{\rm a}$ is the orientation relaxation time. For typical nematics, $D_{\rm a} \sim 4 \times 10^{-2}$ cm^2 s^{-1} and $\tau_{\rm a} \sim 10^{-7}$ c, so $l_{\rm a} \sim 0.6$ μm. The relaxation of director fluctuations is described by the equation

$$\tau_{\rm eff} \cong \tau_{\rm a} \frac{L_{\rm a}^2}{\xi_0^2} \left[1 + l_{\rm a}^2 L_{\rm a}^{-2}\right]^{-1} . \tag{7.29}$$

Since the length ξ_0 is related to the coefficient of elasticity K and the time $\tau_{\rm a}$ to the rotational viscosity coefficient γ_1 [123, 124] as

$$K = \frac{3\rho k_{\rm B} T}{m} S^2 \xi_0^2 , \tag{7.30}$$

$$\gamma_1 = \frac{3\rho k_{\rm B} T}{m} S^2 \tau_{\rm a} , \tag{7.31}$$

expression (7.29) can be reduced to

$$\tau_{\rm eff} \cong \frac{\gamma_1 L_{\rm a}^2}{K} \left[1 + l_{\rm a}^2 L_{\rm a}^{-2}\right]^{-1} . \tag{7.32}$$

Apart from the coefficient π^{-2}, expression (7.32) differs from the expression for the uniform orientation relaxation time (7.12) by the factor

$$\frac{L_{\rm a}^2}{L^2} \left[1 + \frac{l_{\rm a}^2}{L_{\rm a}^2}\right]^{-1} .$$

On condition that $L = L_{\rm a} = l_{\rm a} = 10$ μm, the relaxation time for nonuniform orientation is two times shorter than that for uniform orientation (the effect of nonuniformity at $l_{\rm a} \approx 0.6$ μm is of order 0.5%).

The influence of boundary conditions on the measured viscosity was also examined in [125]. At a finite adhesion energy W characterized by the dimensionless parameter $g = WL/2K_{22}$, Eqn (7.2) for NLC reorientation should be supplemented by the equation for the tilt angle θ, which takes into account the LC orientation at the substrates (the alignment angle and surface energy at coordinates $z = \pm L/2$):

$$K_{22} \left.\frac{\partial^2 \theta}{\partial z^2}\right|_{\pm L/2} \pm W \sin\theta\left(\pm\frac{L}{2}\right) \cos\theta\left(\pm\frac{L}{2}\right) = \gamma_1 \frac{\partial\theta(\pm L/2)}{\partial t} . \tag{7.33}$$

It turned out that a decrease in the parameter g^{-1} increases both the switching-on and the switching-off time. A decrease in g from 10000 to 5 results in a 1.4-fold increase in the effective values of both times. A further decrease in g to 2 caused a 2-fold increase in these effective values [125].

An interesting method allowing one to obtain five coefficients of viscosity $\alpha_1, \ldots, \alpha_5$ was proposed in [126, 127]. The interference of two intense light beams in an LC volume created a spatially periodic structure due to the excitation of acoustic waves and heating. Because of resulting modulation of the NLC refractive index, the diffractional efficiency of the obtained phase grating can be varied using a low-intensity light beam. The relaxation time of the diffractional efficiency is determined by the NLC viscosity and elasticity coefficients. Five combinations of viscosity coefficients can be obtained depending on the director orientation with respect to the polarization of the exciting radiation and probing beam. Ref. [127] describes the limitations on the times of physical processes in LCs, along with the equations of NLC hydrodynamics for the case under consideration. Accurate values of the viscosity coefficients can be obtained if the light pulse duration $\tau_{\rm imp}$ is small compared with the heat transfer times determined by the speed of sound $\tau_{\rm s} \sim v_{\rm s}^{-1}$ and the thermal conduction $\tau_T \sim \varkappa^{-1}$. The influence of thermal conductivity on sound generation should be neglected ($\tau_{\rm s} \ll \tau_T$). The time of sound attenuation due to viscosity should be comparable to the time necessary for a constant temperature to be established ($\tau_v \sim \tau_T$). All these processes should not affect the relaxation of NLC orientation to an equilibrium state under the action of the Frank elastic forces ($\tau_{\rm F} = \gamma_1 q^2/K_{11} \gg \tau_T$). Thus, the relaxation times for the NLC orientation can be obtained if the laser pulse length $\tau_{\rm imp}$ is chosen to be 50 ns or so. At $\tau_{\rm imp} \sim \tau_v \sim 1$ ms, acoustic waves are also excited in the NLC volume, and their attenuation depends on a different combination of viscosity coefficients. The direct effect of the light-wave electric field can be eliminated by a proper choice of the polarization direction relative to the director. If the polarization of the exciting wave is parallel to the director (e – e), the extraordinary sounding wave transforms into the extraordinary wave by scattering (e → e), and the director is parallel to the wave vector of the resultant thermal lattice $\mathbf{q}$ (angle $\angle(\mathbf{n}, \mathbf{q}) = 0$), then η_1 and α_2^2/γ_1 are measured. For the same polarization directions of the exciting and sounding waves, but with $\angle(\mathbf{n}, \mathbf{q}) = 45°$, the coefficients γ_1 and $(\alpha_2/2 + \gamma_2 - \eta_1)$ are measured. The value of $\eta_1 + \eta_3$ can be obtained if $\angle(\mathbf{n}, \mathbf{q}) = 45°$, the director and the exciting wave polarization are mutually perpendicular (e – o), and the ordinary sounding wave converts by scattering into the extraordinary wave (o → e). Thus, all the Leslie viscosity coefficients can be found using this method.

An LC reorientation can be induced by a light wave alone. If a polarized beam of light propagates in an LC cell parallel to the director, this results in a nonlinear phase difference at

the cell outlet, provided the light intensity I exceeds the threshold value I_F for the Freedericksz optical transition. The dynamics of the phase lag $\Phi(t)$ at $I > I_F$ was considered in [128]. Ref. [129] describes a method for the measurement of the viscoelastic ratio K_{33}/η_B with the use of the Freedericksz optical transition. The time dependence of $\Phi(t)$ is described by the expression

$$\Phi(t) = \frac{\Phi_E}{1 + (\Phi_E - \Phi_0)\exp(-2\Gamma_T t)/\Phi(t)}, \tag{7.34}$$

where $\Gamma_T = (K_{33}/\eta_B)(\pi/L)^2(I/I_F - 1)$, and Φ_E and Φ_0 stand for the phase lag at a light intensity slightly above the threshold and for the so-called linear phase lag, respectively. Ref. [129] gives the following expressions for these lags:

$$\Phi_E = \frac{\omega}{2c\varepsilon_\perp^{1/2}} \frac{\varepsilon_a L}{1 - 9\varepsilon_a/4\varepsilon_{||} - (K_{33} - K_{11})/K_{33}} \left(\frac{I}{I_F} - 1\right), \tag{7.35}$$

$$\Phi_0 = \frac{\omega L \varepsilon_a}{4c\varepsilon_\perp^{1/2}} \theta_0^2, \tag{7.36}$$

where ω and c are the frequency and velocity of light, respectively, $\varepsilon_{||}$ and $\varepsilon_\perp$ are the components of the dielectric permittivity at optical frequencies, L is the LC cell thickness, K_{11} and K_{33} are the coefficients of elasticity, and θ_0 is the fluctuation angle of optical axis deviation at which a type-2 phase transition is initiated. By recording transmittance extrema in the case of excitation and relaxation of an homeotropically oriented cell, it is possible to find the viscoelastic ratio K_{33}/η_B from the slope of the dependence $\ln \Phi(t)$ [129].

Until now we have considered the reorientation of a homogeneous LC sample subject to a field strictly perpendicular or parallel to the substrate plane. However, since the director alignments $\mathbf{n}$ and $-\mathbf{n}$ are equivalent, there are two equivalent reorientation directions with tilt angles θ and $\pi - \theta$. Regions with different tilt angles are separated by so-called inversion walls. Even a small tilt of the magnetic field relative to the perpendicular to the substrate plane (angle φ) results in different reorientation angles on the two sides of the wall and leads to its migration (displacement). Leger [130] demonstrated that the wall migration time is directly proportional to the rotational viscosity coefficient γ_1 and inversely proportional to the magnetic field. From the wall migration rate, she obtained γ_1 values for MBBA (0.86 ± 0.2 Pa) and PAA (0.08 ± 0.02 Pa), which are consistent with those previously reported. Ref. [131] examines inversion wall movements at greater length. Their migration rate v is described by the relation

$$v = \frac{3\sqrt{3}\,\pi\varphi K_{11}^{\text{eff}} q}{8\gamma_1^{\text{eff}} L(H/H_{cr} - 1)}, \tag{7.37}$$

where γ_1^{eff}, K_{11}^{eff} are the effective coefficients of viscosity and elasticity, respectively, and φ is the tilt angle of the magnetic field (near the Freedericksz transition threshold at $H/H_{cr} = 1.1$, $\varphi < 3.9^\circ$ and $q = 3\varphi \sin\theta_{max}/4\theta_{max}^4$; θ_{max} is the tilt angle of the director in the middle of the LC layer). For a MBBA-containing sample ($\gamma_1^{\text{eff}} = 0.85\gamma_1$, $\gamma_1 = 0.76$ Pa, $K_{11} = 6 \times 10^{-7}$ dyn) of thickness $L = 100$ μm, at $\varphi \sim 5^\circ$, the velocity v calculated by X Wang at different H/H_{cr} values using formula (7.37) is in good agreement with the experimental findings of L Leger. Migrations of the inversion walls in nematics is a good model for signal propagation in a nerve, whose myelin sheath has a liquid-crystal structure. In both cases, the velocity of motion is described by similar equations

$$\frac{\partial v}{\partial t} = \frac{\partial^2 v}{\partial x^2} + f(v) \tag{7.38}$$

[cf. (7.10)].

Another example of the coexistence of two types of orientations under identical boundary conditions is provided by nematic twist cells. In the case of mutually orthogonal director orientations at opposite substrate plates in the absence of chiral additives, both right- and left-hand-twisted states of the director are possible. This in turn gives rise to domains twisted by $\pm 90^\circ$ and separated by disclinations. The velocities of their motion depend on the local radius of curvature and are described by an expression analogous to (7.37) [132, 133]:

$$v = C\frac{K_{11}}{\gamma_1}\frac{1}{R} = \frac{\Gamma}{R}, \tag{7.39}$$

where Γ is the kinetic coefficient, which can be found from the time dependence of the radii of curvature of disclination loops [134]. In experiment, the loops are observed with a microscope to directly obtain R values or to find the correlation function describing the relaxation of the regions of right- and left-hand-twisted states (with respect to the initial pattern that appears in a twist cell upon an isotropic–nematic phase transition). In either case, the measured parameter is proportional to $(\Gamma t)^{1/2}$ because of the time dependence of the disclination length. This regularity can be found by applying the u-field theory [135] which describes an 'order–disorder' transition in a system of random interfaces between two stable phases.

Ref. [136] reports an experiment whose geometry corresponds to the T-effect [111]. A 25 to 250 μm thick planar oriented cell is placed between the poles of a magnet so that the field is oriented parallel to the director. Thereafter, the cell is rapidly (within a time less than the orientation relaxation time) turned through a right angle. Also, a transverse magnetic field may be switched on. As a result, a periodic pattern (so-called twist-bend walls) arises in the bulk of the LC. According to [137], the wall period is related to the magnetic field intensity B, which should be slightly higher than the threshold Freedericksz transition B_F, and also to the viscosity and elasticity coefficients of the NLC, by the following expression:

$$\left(\frac{B}{B_F}\right)^2 = \left(\frac{1-\alpha}{\eta\alpha}k\right)Q^4 + \frac{2k}{\alpha}Q^2 + \frac{1+k\eta}{\alpha}, \tag{7.40}$$

where Q is the cell-to-wall wave vector ratio, $Q = q_x/(\pi/L) = 2L/\lambda$, λ is the average wall period, $\alpha = \alpha_2^2/\gamma_1\eta_1$, $\eta = \eta_1/\eta_3$, and $k = K_{33}/K_{22}$. Ref. [136] also reports the viscosity coefficient ratios $\alpha = 0.86$ and $\eta = 0.23$ obtained by the best fit method for a Mi-5 mixture available from Merck.

A comparison of the methods described in this section demonstrates that they all require much less LC than the rotating magnetic field method. This is an important advantage in the context of evaluation of new LC substances. Moreover, the work can be done using simpler

instruments without a substantial loss in accuracy. Optical methods should be preferred to avoid serious errors that may result from field and thickness inhomogeneities in capacitance measurements. Moreover, an electric field should be applied wherever possible because it is very difficult to directly measure the anisotropy of diamagnetic susceptibility χ_a [3].

8. Light scattering techniques

Local fluctuations $\delta\mathbf{n}$ of the director $\mathbf{n}$ result in intense light scattering and turbidity of the LC sample. The theory the statics and dynamics of director fluctuations in NLCs is developed in [138, 139]. It is also comprehensively dealt with in a few books [2, 3, 87]. We therefore confine ourselves to the description of certain practically important experiments [140 – 146].

For the purpose of the analysis of fluctuations $\delta\mathbf{n}$ of the director $\delta\mathbf{n}$, it is convenient to decompose $\delta\mathbf{n}$ into two mutually perpendicular components (modes). One of them, $\delta\mathbf{n}_1$, represents the superposition of bend and splay elastic deformations, while the other, $\delta\mathbf{n}_2$, is a combination of bend and twist deformations. We write down expressions for the intensity and half-width of the scattered light spectra for each mode, using [139]. The light scattering intensity is determined by the expression for the scattering cross section

$$\sigma = \sum_{\alpha=1,2} \frac{(i_\alpha f_0 + i_0 f_\alpha)^2}{K_{33} q_{||}^2 + K_{22} q_\perp^2}\,, \tag{8.1}$$

where i_α, f_α are the projections of the polarization vectors of incident (**i**) and scattered (**f**) light onto orts $\mathbf{e}_\alpha$ chosen in the following way: $\mathbf{e}_1 \perp \mathbf{n}$, and $\mathbf{e}_1$ lies in the plane of the director $\mathbf{n}$ and the scattering wave vector $\mathbf{q} = \mathbf{k}_i - \mathbf{k}_s$ ($\mathbf{k}_i, \mathbf{k}_s$ are the wave vectors of incident and scattered light, respectively); $\mathbf{e}_1 \perp \mathbf{e}_2$, and $\mathbf{e}_1$ is perpendicular to the plane of vectors $\mathbf{n}, \mathbf{q}$; $i_0 = (\mathbf{in})$, $f_0 = (\mathbf{fn})$; K_{ii} are the Frank elastic constants; $q_{||}$ and $q_\perp$ are the components of the scattering wave vector with respect to the direction of $\mathbf{n}$ (Fig. 20). The expression for the intensity of the light scattering spectrum has the form [146]

$$S_{\Delta I}(\omega) = \beta^2 \left\{ \sum_{\alpha=1,2} \frac{G_\alpha^4(\theta) 2u_\alpha}{K_\alpha^2(q)[\omega^2 + 4u_\alpha^2]} + \frac{G^2 G_\alpha^2(\theta)(u_1 + u_2)}{K_1 K_2(q)\left[\omega^2 + (u_1 + u_2)^2\right]} \right\}, \tag{8.2}$$

where u_α is the scattering spectrum half-width and β is a function of the dielectric anisotropy at optical frequencies (refractive indices), scattering volume, distance to the observation point, and absolute temperature T. The transfer equations for different director fluctuation modes ($\delta n_\alpha(\mathbf{q}) \ll 1$) in the above coordinate system have the form

$$\frac{\partial}{\partial t}\,\delta n_\alpha(\mathbf{q}) + \frac{1}{\tau_\alpha}\,\delta n_\alpha(\mathbf{q}) = 0\,, \quad \alpha = 1, 2\,. \tag{8.3}$$

Here, τ_α denotes relaxation times

$$\tau_\alpha(q) = \frac{\eta^{\text{eff}}(\mathbf{q})}{K_\alpha(\mathbf{q})}\,. \tag{8.4}$$

For the effective viscosity coefficient, the angular dependences are described by the relations

$$\eta_1^{\text{eff}}(\mathbf{q}) = \gamma_1 - \frac{\left(\alpha_3 q_\perp^2 - \alpha_2 q_{||}^2\right)^2}{\eta_2 q_\perp^4 + (\eta_1 + \eta_2 + \eta_{12}) q_\perp^2 q_{||}^2 + \eta_1 q_{||}^4}\,, \tag{8.5}$$

$$\eta_1^{\text{eff}}(\mathbf{q}) = \gamma_1 - \frac{\alpha_2 q_{||}^2}{\eta_3 q_\perp^2 + \eta_1 q_{||}^2}\,; \tag{8.6}$$

for the elasticity coefficient, by the relation

$$K_\alpha(\mathbf{q}) = K_{\alpha\alpha}\, q_\perp^2 + K_{33}\, q_{||}^2\,. \tag{8.7}$$

Formulas (8.5), (8.6) can be substantially simplified assuming that $q_{||} \gg q_\perp$ or $q_\perp \gg q_{||}$.

In the former case,

$$\frac{K_{33} q_{||}^2}{u} = \eta_B = \gamma_1 - \frac{\alpha_2^2}{\eta_1}\,. \tag{8.8}$$

for both decaying modes. If $q_\perp \gg q_{||}$, we have for mode 1

$$\frac{K_{11} q_\perp^2}{u_1} = \eta_S = \gamma_1 - \frac{\alpha_3^2}{\eta_2}\,, \tag{8.9}$$

and for mode 2

$$\frac{K_{22} q_\perp^2}{u_2} = \gamma_1\,. \tag{8.10}$$

Here, u_i are the half-widths of the scattering spectra (rad s^{-1}) related to the characteristic time of the scattered light correlation function by the equation $2u_i = \tau_i^{-1}$, while η_S and η_B have the same meaning and form as in expressions (7.8) and (7.9). As a rule, u_i values range from 10 to 1000 rad s^{-1}, and light beating spectroscopy should be used for their accurate determination [147].

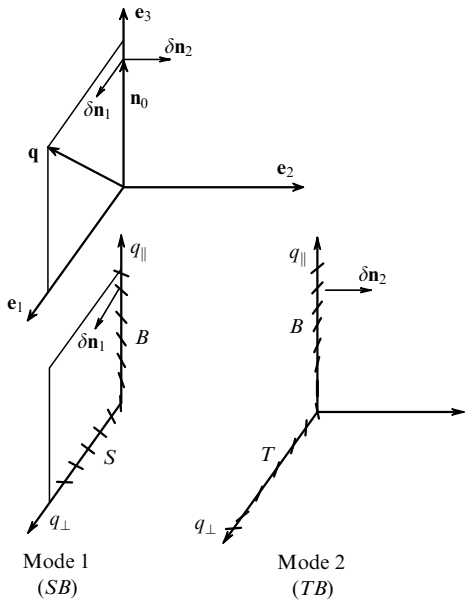

Figure 20. The construction of the basis orthogonal unit vectors $\mathbf{e}_1$, $\mathbf{e}_2$, $\mathbf{e}_3$ (using the wave vector and director $\mathbf{n}$) in which two noncorrelated fluctuation modes $\delta\mathbf{n}_1$ and $\delta\mathbf{n}_2$ are expanded, and the director orientation in these modes.

The noise excess over the background, due to light scattering by director thermal fluctuations, is for the heterodyne spectrum (measured by mixing the scattered light with a local oscillator — originally split laser beam) twice as high as that for the homodyne spectrum. Due to the Gaussian character of fluctuations, the half-width of the heterodyne spectrum is one half as large as that of the homodyne spectrum [142].

It follows from formula (8.2) that the scattering spectrum consists of three Lorentzian lines with slightly different half-widths. The spectral half-width can be measured more accurately if we determine the frequency at which $\omega S_{\Delta I}(\omega)$ is maximum [146]. For a purely Lorentzian spectrum, $\omega_{\max}$ coincides with the half-width $\omega_{1/2}$. The dependence $\omega_{1/2}(q_\perp^2)$ is shown in Fig. 21. The relative error of measuring the viscoelastic ratio in this way amounts to 2%, and the K_{11}/K_{22} ratio does not significantly influence the fitting procedure.

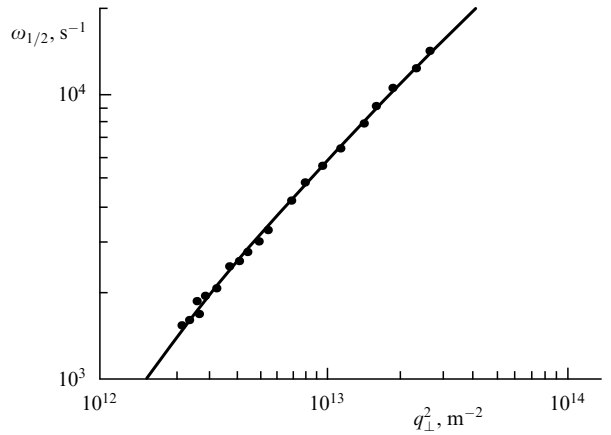

Figure 21. Half-width $\omega_{1/2}$ of the scattering spectrum versus squared wave vector $q_\perp^2$ for $CH_3-C_6H_4-CH=N-C_6H_4-OCO-CH_3$ ($\tau = 0.9988$). The solid line represents the results of data treatment in compliance with the condition $(dS/d\omega)_{\omega=\omega_{1/2}} = 0$ [146].

An electric field applied to the cell does not change the shape of the scattering spectrum for mode 2 (twist-bend mode), and the line width increases in proportion to the applied voltage squared. The value of $S_{\Delta I}(\omega)$ for mode 1 lies slightly below the level determined by the Lorentzian shape, probably due to the effect of electrical conduction [148].

A schematic diagram of the experimental arrangement for measurements of the scattering spectrum is shown in Fig. 22. A polarized laser beam scattered from an LC sample at an angle θ is sent to a photodetector and thereafter enters a pulsed analog correlator that determines the correlation function of photon fluctuations. In the case of light scattering by a single fluctuation mode, the correlation function has the form $\rho(t) \sim \exp(-t/\tau)$. Figure 23 depicts optical geometries for the observation of light scattering by decaying *S*- and *B*-modes. The laboratory scattering angles θ_α are calculated based on the known refractive indices of the given NLC so that one of the components of vector **q** vanish. For the geometry shown in Fig. 23a, $k_i = 2\pi n_o/\lambda$, $k_s = 2\pi n_e/\lambda$ (n_o and n_e are the refractive indices of ordinary and extraordinary beams, respectively), $q_{||} = 0$, and the laboratory angle for MBBA is $\theta_1 = 56°$ [143]. It follows from the comparison of Figs 23b and 23c that the transition from the geometry in which light is scattered by the B-mode to the scattering

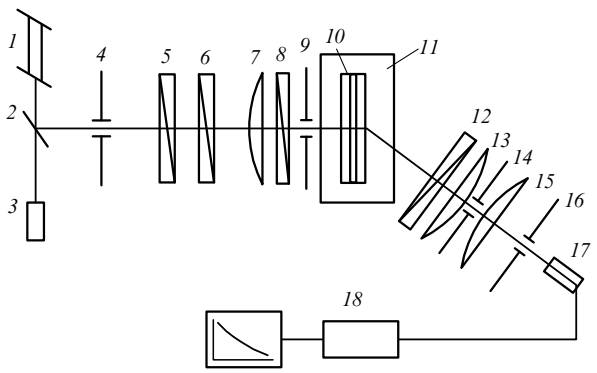

Figure 22. Schematic of the experimental arrangement for measuring the viscoelastic characteristics of NLCs with the use of photon correlation spectroscopy: *1*, laser; *2*, beam splitter; *3*, *17*, photodetectors; *4*, *9*, *14*, *16*, diaphragms; *5*, *8*, *12*, polarizers; *6*, quarter-wave plate; *7*, lens improving the spatial coherence of the beam; *10*, LC cell; *11*, oven; *13*, *15*, collimator lenses; *18*, correlometer.

geometry involving the S-mode is achieved by a 90° rotation of the NLC sample.

Let us scrutinize the experimental geometry presented in Fig. 23b in which the vector **i** is parallel to the director **n** and perpendicular to the scattering plane determined by the wave

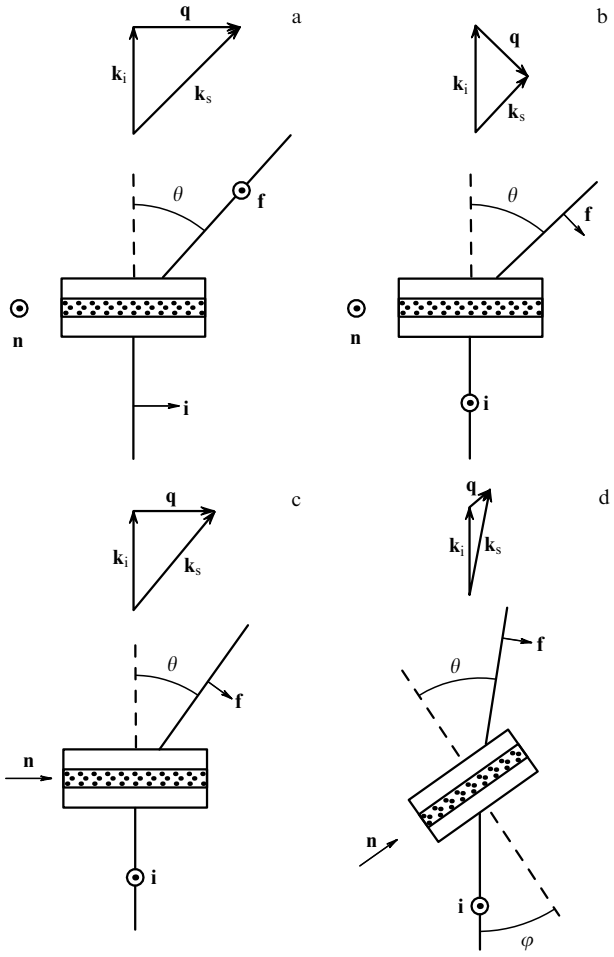

Figure 23. Optical geometries for the observation of light scattering by (a, b) a damped *S*-mode and (c, d) damped *B*-modes [143].

vectors $\mathbf{k}_i$ and $\mathbf{k}_s$. In this case, $k_i = 2\pi n_e/\lambda$, $k_s = 2\pi n_o/\lambda$, $q_{||} = k_s \sin\theta$, $q_\perp = = k_i - k_s \cos\theta$; for small scattering angles, as $\theta \to 0$ (and $q_{||} \to 0$), light is scattered by mode 2, whose dynamics is described by expression (8.10). However, the accuracy of measuring γ_1 for such a geometry is low because of the strong parasitic scattering from defects of sample ordering (especially in the 'forward' direction). Nevertheless, using light beating spectroscopy and measurements at different scattering angles θ, the viscoelastic ratios γ_1/K_{22} and η_S/K_{11} can be obtained with a fairly good accuracy [145]. For an arbitrary angle θ, the scattered light spectrum is a superposition of two Lorentzian lines, and the scattered light correlation function is a superposition of two exponents. The normalized correlation function can be written in the following way:

$$\rho(t) = \frac{a_1 \exp(-t/\tau_1) + a_2 \exp(-t/\tau_2)}{a_1 + a_2}\,;$$

$$a_\alpha = \frac{G_\alpha^2}{K_\alpha(q)}\,, \qquad \alpha = 1, 2\,, \tag{8.11}$$

where $G_\alpha = i_0 f_\alpha + i_\alpha f_0$ is the scattering geometry factor for modes 1 and 2, and $K_\alpha(q) = K_{\alpha\alpha} q_\perp^2 + K_{33} q_{||}^2$. It is convenient to determine the slope of the asymptote of $\ln \rho(t)$:

$$\tau_{\text{eff}}^{-1} = \frac{\mathrm{d}}{\mathrm{d}t}\big(-\ln\rho(t)\big)\bigg|_{t=0} \left(\frac{a_1}{\tau_1} + \frac{a_2}{\tau_2}\right) \frac{1}{a_1 + a_2}\,. \tag{8.12}$$

For the geometry of the arrangement under consideration, Eqn (8.12) reduces to

$$\tau_{\text{eff}}^{-1} = q_\perp^2 \, \frac{G_1^2/\eta_S + G_2^2/\gamma_1}{G_1^2/K_{11} + G_2^2/K_{22}}\,. \tag{8.13}$$

Taking into account that $\eta_S \cong \gamma_1$ and $G_1^2 + G_2^2 = 1$, Eqn (8.13) can be transformed into

$$\tau_{\text{eff}}\, q_\perp^2 = \frac{\gamma_1}{K_{22}} \left[\left(\frac{K_{22}}{K_{11}} - 1\right) G_1^2 + 1\right]. \tag{8.14}$$

Expression (8.14) describes well the measured dependences of the relaxation time τ_{eff} on G_1, which is a function of the scattering angle for two NLCs. The relation $\eta_S \cong \gamma_1$ is satisfied fairly well. For these substances, γ_1/K_{22} and γ_1/K_{11} values can be obtained at $G_1 = 0$ and $G_1 = 1$, respectively.

For the experimental geometry shown in Fig. 23c (where both the incident light polarization and the director are parallel to the scattering plane), it is possible to determine η_B/K_{33}, γ_1/K_{33}, and the Miesowicz coefficient ratio η_1/η_3 [146]. The measured spectrum half-width $\Delta\omega_{1/2}$ is linked to the measurement angles via the following expression, which takes into account (8.4) and (8.8):

$$B(\mathbf{q}) = \frac{2(q_{||}^2 + K_{22} q_\perp^2/K_{33})}{\Delta\omega_{1/2}} = \frac{1}{K_{33}} \left[\frac{1}{2}\,(\gamma_1 + \eta_B) + \frac{1}{2}\,(\gamma_1 - \eta_B) Z(\mathbf{q})\right], \tag{8.15}$$

where

$$Z(\mathbf{q}) \equiv \left(\frac{\eta_3}{\eta_1}\, q_\perp^2 - q_{||}^2\right) \left(\frac{\eta_3}{\eta_1}\, q_\perp^2 + q_{||}^2\right)^{-1}. \tag{8.16}$$

At $Z = 1$ ($q_{||} = 0$) $B = \gamma_1/K_{33}$, and at $Z = -1$ ($q_\perp = 0$) $B = \eta_B/K_{33}$. The ratio η_1/η_3 can be found either by adjusting the dependence $B(Z, u_s, K_{22}/K_{33})$ or from the slope of the dependence

$$C(q) \equiv \frac{B(q) - B_{Z=-1}}{B(q) - B_{Z=1}} = -\frac{\eta_3 q_\perp^2}{\eta_1 q_{||}^2}\,.$$

It should be recalled that $\eta_1/\eta_3 \equiv \eta_S/\eta_B$ [see (3.9)].

If there is a spatial nonuniformity of the director of characteristic length l_a, the line width of the scattering spectrum increases in proportion to $1 + l_a^2 q^2$ [123]. The analogous expression for the deformation induced by an external field is (7.32).

The foregoing discussion in of this section concerned the normal light incidence on the cell. In Refs [149, 150], the characteristic relaxation times were calculated and measured for different incidence and scattering angles. This approach significantly broadens the range of angles for which $q_\perp/q_{||} \ll 1$ or $q_{||}/q_\perp \ll 1$ and allows the number of measured viscosity coefficients to be increased by fitting experimental data to relevant approximations. Figure 24 illustrates the measurement of incidence and scattering angles in a liquid-crystal medium (φ, θ) and in air (φ', θ') for homeotropic and planar orientations. In both cases, the director is in the scattering plane.

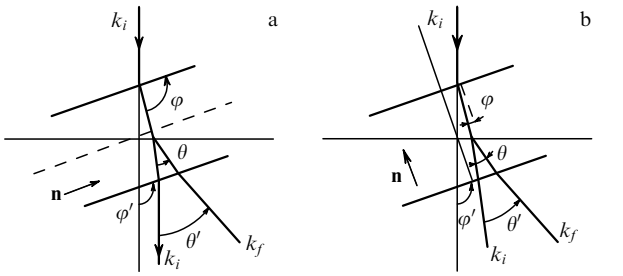

Figure 24. Light incidence angles relative to the director in a liquid crystal and in air (φ and φ' respectively) and scattering angles in a liquid crystal and in air (θ, θ') for (a) planar and (b) homeotropic director orientations at the substrate plates [149].

The dependences of the width τ_α^{-1} of the scattering spectrum calculated for the homeotropic orientation of the NLC over the ranges $-90° \leqslant \varphi \leqslant 90°$ and $0 \leqslant \theta \leqslant 180°$ have a center of symmetry at the point with coordinates $\varphi = 0$, $\theta = 0$ and an angular period of 180° [150]. For $|\varphi| \leqslant 30°$ and $\theta \sim 20-40°$, which is normally the case in experiment, the quantity τ_α^{-1} is of the order of 10 kHz. At a constant scattering angle θ, the dependence $\tau(\varphi)$ has a nonmonotonic form. This finding is confirmed by the results of measuring the inverse of the relaxation time as a function of the incidence angle at different scattering angles in air for homeotropic and planar orientations. The line width for geometries e – o and o – e is smaller than for polarized scattering (e – e); that is, both the corresponding relaxation times and the recorded light scattering intensities are smaller. This means that the incident light intensity should be increased to improve the accuracy of line width measurements in the case of scattering depolarization.

The choice of the geometrical arrangement for measuring the viscosity coefficients is illustrated by Fig. 25 [150]. The dashed lines correspond to zero Rayleigh scattering intensity I^α and are not suitable for the solution of the problem in question. They are described by the following equations:

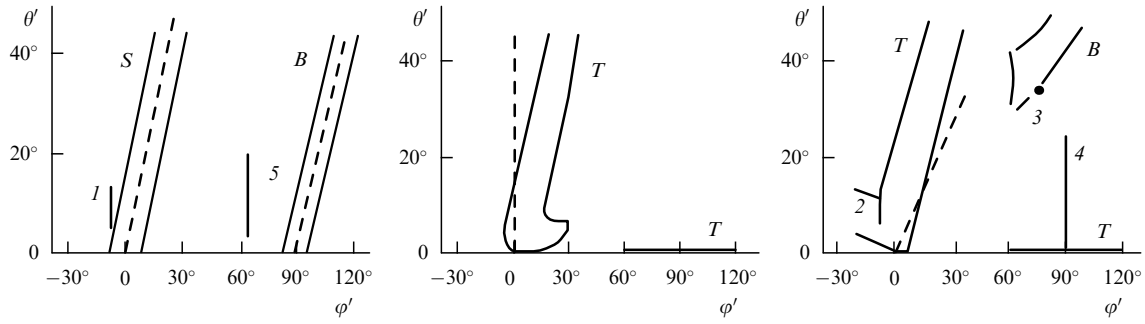

Figure 25. Incidence (φ') and scattering (θ') angles for different modes in which the director fluctuations are determined by *S*-, *B*-, and *T*-deformations: dashed lines, $I^{\alpha} = 0$; *1–5*, scattering geometries recommended for measuring combinations of the Leslie viscosity coefficients [150].

$$\varphi' = \frac{\theta'}{2} \quad \text{(homeotropic orientation)},$$

$$\varphi' = \frac{\theta'}{2} + 90^\circ \quad \text{(planar orientation)},$$

$$\varphi' = 0 \quad \text{(homeotropic orientation)},$$

$$\varphi' = \theta' \quad \text{(homeotropic orientation)}.$$

For measuring η_S and γ_1, $\varphi' = -8^\circ$, $5^\circ \leqslant \theta' \leqslant 10^\circ$, and homeotropic orientation are recommended (polarized light scattering (e–e) in the former and depolarized scattering (o–e) in the latter cases; see lines *1* and *2* in Fig. 25). The quantity η_B can be measured at $\varphi' = 73^\circ$, $\theta' = 34^\circ$ in a planar oriented cell if the incident light polarization is perpendicular to the director (o–e; point *3* in Fig. 25). The line width of the scattering spectrum significantly increases with small changes in the scattering angle. By properly choosing the scattering geometries and mathematically treating the results, it is possible to obtain viscoelastic ratios for almost all Leslie viscosity coefficients. The measurements of the relaxation time using lines *4* ($\varphi' = 90^\circ$, $0 \leqslant \theta' \leqslant 28^\circ$) and *5* ($\varphi' = 65^\circ$, $2^\circ \leqslant \theta' \leqslant 19.7^\circ$) in Fig. 25 yielded estimates for the quantity $\alpha_4/2\alpha_2^2$ and the coefficient α_1 respectively.

It was demonstrated in [151] that a Lorentzian-shaped spectrum can be obtained even for very small scattering angles (0.015 rad $\sim 1^\circ$) using a homeotropically aligned NLC and oblique incidence, because of the reduction of the multiple scattering intensity. This spectrum can be distinguished quite reliably against the background of static scattering using the homodyne method. As a result, the ratio γ_1/χ_a or η_S/χ_a and η_B/χ_a can be determined instead of the viscoelastic ratio because in this case, since the wave vector is small, the denominator of (8.4) contains the term $K(q) + \chi_a H^2$, which describes the magnetic field and prevails due to the smallness of the wave vector q.

Using Raman light scattering in an NLC sample subject to an electric field makes it possible to find the relaxation times separately for the rigid backbone of the original molecules and for their more flexible alkyl substitutes. This approach is described in [152].

Although the measurement of the viscoelastic ratios by light scattering techniques requires sophisticated instrumentation and specially equipped laboratories, it provides highly valuable scientific information, since experiments are performed on intact liquid crystals and are free of many errors intrinsic in other methods. The amount of the analyte may be very small (30–50 mg). Also, the dependence of the rotational viscosity γ_1 on temperature and on the degree of regularity can be exactly estimated.

9. Conclusion

Figure 26 represents the results of measuring the temperature dependence of γ_1 for BF-5 by three different methods [153]. Good agreement between them testifies to the validity of the techniques employed.

Our analysis of the reviewed investigations has demonstrated the paramount importance of the correct determination of boundary conditions, velocities of the LC flow or rotation, and the external field, as well as of the proper choice of the signal detectors. The shear flow technique appears to provide the most comprehensive information about all coefficients, but it requires a large amount of the analyte.

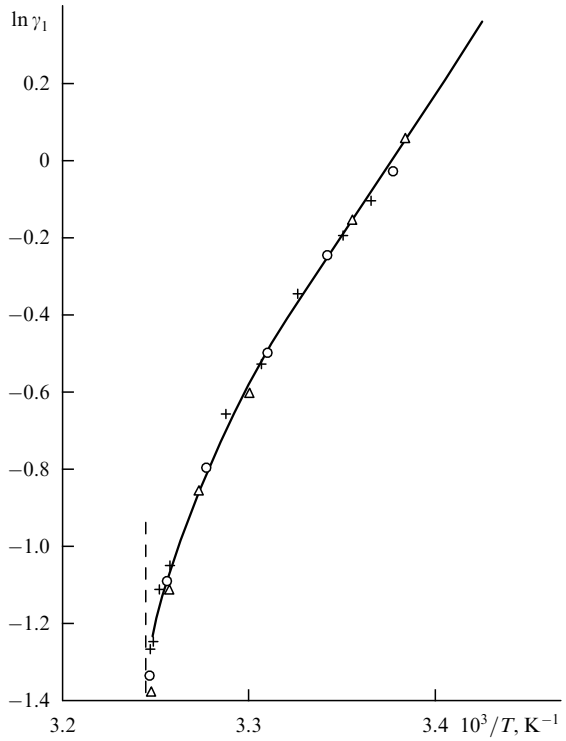

Figure 26. Temperature dependences of the rotational viscosity coefficient γ_1 (poise) for pentylcyanobiphenyl measured by the rotating magnetic field method (o), the light scattering technique (Δ), and from the relaxation of the Freedericksz transition optical response (+) [153].

Table 2. Viscosity coefficients of NLCs and methods for their measurement.

Notation for the viscosity coefficient	Relation to other viscosity coefficients	Name	Measuring technique	
$\alpha_i\ (i=1,\ldots,6)$	—	Leslie viscosity coefficients	—	
η	$\sim\eta_2-\alpha_3\sim\eta_2$ $(-\alpha_2\gamma_2/\gamma_1+\alpha_4+\alpha_5)/2$	Dynamic viscosity	Capillary or rotational viscometer Ultrasonic shear	
ν	η/ρ	Kinematic viscosity	Capillary viscometer	
η_1	$(-\alpha_2+\alpha_4+\alpha_5)/2$	Miesowicz viscosity coefficients	Poiseuille or Couette flow	$\mathbf{v}\perp\mathbf{n}$, $\mathbf{n}\,\|\|\,\nabla\mathbf{v}$
η_2	$(\alpha_3+\alpha_4+\alpha_6)/2$			$\mathbf{v}\,\|\|\,\mathbf{n}$, $\mathbf{n}\perp\nabla\mathbf{v}$
η_3	$\alpha_4/2$			$\mathbf{v}\perp\mathbf{n}$, $\mathbf{n}\perp\nabla\mathbf{v}$
η_{12}	α_1			$\angle(\mathbf{v},\mathbf{n})=45^\circ$
γ_1	$\alpha_3-\alpha_2$	Rotational (Tsvetkov) viscosity coefficient	Rotating magnetic field method Freedericksz transition dynamics Light scattering from thermal fluctuations of the director	
γ_2	$\alpha_3+\alpha_2$	Twist deformation constant in a velocity gradient	Couette flow	
η_S	$\gamma_1-\alpha_3^2/\eta_1$	Splay viscosity coefficient	Freedericksz transition dynamics Light scattering from thermal fluctuations of the director	
η_B	$\gamma_1-\alpha_2^2/\eta_2$	Bend viscosity coefficient	Freedericksz transition dynamics Light scattering from thermal fluctuations of the director	

The complete set of viscosity coefficients is obtainable by measuring light scattering from thermal fluctuations of the LC director. This approach requires only a small amount of the LC substance, but the experiment cannot be done without special instruments. The method evaluating the relaxation of the Freedericksz transition is simple and also requires a small amount of the LC for analysis.

The dynamic responses of LCs can be most conveniently studied using optical methods. Acoustic methods, especially suitable for measurements under high pressure, are also efficient.

To estimate the rotational viscosity, the groups and laboratories employing liquid-crystalline materials in their practice, can use simple Ostwald or Haake viscometers measuring the coefficients of kinematic and dynamic viscosity and analyzing the Freedericksz transition relaxation in planar oriented cells.

Table 2 lists the viscosity coefficients of NLCs and methods for their determination [154]. The reader is also referred to the reviews [155, 156].

The present article was deliberately confined to the description of methods for only nematic LCs, which have the simplest structure and are most widely used in practice. Other phases are, as a rule, characterized by a larger number of viscosity coefficients, which are measured by different methods. A detailed discussion of this problem requires in a special review.

The effect of the molecular structure on the viscosity of nematic LCs was studied in [157, 158]. These works report detailed experimental data and offer their theoretical interpretation.

I cordially thank all the people who benefited the preparation of this review. These are L M Blinov, the founder of the Russian school of experimental electrooptical liquid crystal research, M F Grebenkin, V G Chigrinov, S A Ivanov, A S Sonin, M A Osipov, V N Sadovskiĭ, S Hess, F Schneider, D Danmur, Z Rashewskiĭ, A S Lagunov, D L Bogdanov, S V Pasechnik, and A A Tabidze. At different periods of my life, I was brought together with these people, who actively participated and still participate in the development of the contemporary science of liquid crystals. They willingly shared their knowledge and experience with me, frequently provided me with their works prior to publication, and displayed their persistent interest in and encouragement of the my own ideas. Even more people should be mentioned here whom I have contacted during my work on different aspects of LC viscosity and other physical properties. Special thanks are due to T L Khorunzhenko, of the 'Kometa' R D Center Library, who has compiled a unique bibliographic card index concerning liquid crystals. This enabled me to include many rare publications, which are not readily available, in the present review.

I dedicate this work to the memory of M Miesowicz, V Tsvetkov, and F Leslie, the founders of mesogen viscosity science.

References

1. Blinov L M *Elektro- i Magnitoopticheskie Svoĭstva Zhidkikh Kristallov* (Electro- and Magnetooptic Properties of Liquid Crystals) (Moscow: Nauka, 1977) [Translated into English: *Electro-Optical and Magneto-Optical Properties of Liquid Crystals* (Chichester: Wiley, 1983)]
2. Chandrasekhar S *Liquid Crystals* (Cambridge: Cambridge Univ. Press, 1977) [Translated into Russian (Moscow: Mir, 1980)]
3. de Jeu W H *Physical Properties of Liquid Crystalline Materials* (New York: Gordon and Breach, 1980) [Translated into Russian (Moscow: Mir, 1982)]
4. Grebenkin M F, Ivashchenko A V *Zhidkokristallicheskie Materialy* (Liquid Crystal Materials) (Moscow: Khimiya, 1989)
5. Ericksen J L *Mol. Cryst. Liquid Cryst.* **7** 153 (1966)
6. Leslie F M *Arch. Rat. Mech. Anal.* **28** 265 (1968)

7. Parodi O *J. Phys.* (Paris) **31** 581 (1970)
8. Martin P C, Parodi O, Pershan P C *Phys. Rev. A* **6** 2401 (1971)
9. Forster D et al. *Phys. Rev. Lett.* **26** 1017 (1971)
10. Forster D *Phys. Rev. Lett.* **32** 1161 (1974)
11. Lifshitz E M, Pitaevskiĭ L P, in Landau L D, Lifshitz E M *Teoriya Uprugosti* (Theory of Elasticity) Vol. 7 (Moscow: Nauka, 1987) p. 208 [Translated into English (Oxford: Pergamon Press, 1986)]
12. Pasechnik S V et al. *Zh. Fiz. Khim.* **61** 1675 (1987)
13. Muschik W, Ehrentraut H, Papenfuss C *Mol. Cryst. Liq. Cryst.* **262** 417 (1995)
14. Papenfuss C, Muschik W *Mol. Cryst. Liq. Cryst.* **262** 473 (1995)
15. Ehrentraut H, Muschik W *Mol. Cryst. Liq. Cryst.* **262** 561 (1995)
16. Gaehwiller Ch *Mol. Cryst. Liq. Cryst.* **20** 301 (1973)
17. Miesowicz M *Nature* **136** 261 (1935)
18. Belyaev V V, Nemtsov V B *Zh. Fiz. Khim.* **66** 2763 (1992)
19. Brochard F, Pieranski P, Guyon E *Phys. Rev. Lett.* **28** 1681 (1972); Pieranski P, Brochard F, Guyon E *J. Phys.* (Paris) **34** 35 (1973)
20. Van Doorn C Z *J. Phys. Colloq.* **36** C1-261 (1974)
21. Chigrinov V G, Belyaev V V *Kristallografiya* **22** 603 (1977)
22. Shmelev O Ya et al. *Zh. Fiz. Khim.* **59** 2036 (1985)
23. Kneppe H, Schneider F, Sharma N K *Ber. Bunsenges. Phys. Chem.* **85** 784 (1981); Kneppe H, Schneider F, Sharma N K *J. Chem. Phys.* **77** 3203 (1982)
24. Kneppe H, Schneider F *Mol. Cryst. Liq. Cryst.* **65** 23 (1981)
25. Belyaev V V, Ivanov S A, Grebenkin M F *Kristallografiya* **30** 1160 (1985)
26. Bock F -J, Kneppe H, Schneider F *Liq. Cryst.* **1** 239 (1986)
27. Van der Meulen J P, Zijlstra R J J *Physica B* **132** 153 (1985)
28. Malkin A Ya, in *Fizicheskaya Entsiklopediya* T. 1 (Physical Encyclopaedia Vol. 1) (Moscow: Sovetskaya Entsiklopediya, 1988) p. 283
29. Miesowicz M *Nature* **158** 27 (1946)
30. Tsvetkov V N, Mikhailov G M *Acta Physicochim. URSS* **8** 77 (1938)
31. Miesowicz M *Mol. Cryst. Liq. Cryst.* **97** 1 (1983)
32. Hennel F et al. *Mol. Cryst. Liq. Cryst.* **191** 401 (1990)
33. Tsvetkov V A, Bersenev G A *Prib. Tekh. Eksp.* **5** 223 (1977)
34. Tsvetkov V A *Mol. Cryst. Liq. Cryst.* **52** 208 (1985)
35. Beens W W, de Jeu W H *J. Phys.* (Paris) **44** 129 (1983)
36. Kuz'min N G, Sevost'yanov V P, Filipchenko V Ya, in *Tez. Dokl. 5 Vses. Konf. "Zhidkie Kristally i Ikh Prakticheskoe Ispol'zovanie"* (*Ivanovo, 1985*) T. 2, Kn. 2 (Abstr. 5 All-Union Conf. "Liquid Crystals and Their Practical Applications" (Ivanovo, 1985) Vol. 2, book 2 (Ivanovo: Izd. Ivan. Gos. Univ., 1985) p 71
37. Hess S, Koo H-M *J. Non-Equilib. Thermodyn.* **14** 159 (1989)
38. Derfel G, Radomska B *Proc. SPIE* **3318** 300 (1998)
39. Hunniset S D, van der Sluijs J C A *J. Phys. Lett.* (Paris) **44** L59 (1983)
40. White A E, Cladis P E, Torza S *Mol. Cryst. Liq. Cryst.* **43** 13 (1977)
41. Narasimhan M N L, Eringen A C *Mol. Cryst. Liq. Cryst.* **29** 57 (1974)
42. Atkin A J *Arch. Rat. Mech. Anal.* **38** 224 (1970)
43. Ericksen J L *Trans. Soc. Rheol.* **6** 255 (1969)
44. Fischer J, Frederickson A G *Mol. Cryst. Liq. Cryst.* **6** 255 (1969)
45. Tseng H C, Silver D L, Finlayson B A *Phys. Fluids.* **15** 1213 (1972)
46. Kini U D, Ranganath G S *Pramana* **4** 19 (1975)
47. Tzykalo A L, Shteĭnberg E A, in *Tez. Dokl. 6 Vses. Konf. "Zhidkie Kristally i Ikh Prakticheskoe Ispol'zovanie"* (*Chernigov, 1988*) T. 3 (Abstr. 6 All-Union Conf. "Liquid Crystals and Their Practical Applications" (Chernigov, 1988) Vol. 2 (Chernigov: Izd. Chernigov. Gos. Ped. Inst., 1988) p. 365
48. Leslie F M *Mol. Cryst. Liq. Cryst.* **63** 111 (1981)
49. Benicewicz B C, Johnson J F, Shaw M T *Mol. Cryst. Liq. Cryst.* **65** 111 (1981)
50. Krynkina S V, Molochko V A, in *Tez. Dokl. 5 Vses. Konf. "Zhidkie Kristally i Ikh Prakticheskoe Ispol'zovanie"* (*Ivanovo, 1985*) T. 1, Kn. 2 (Abstr. 5 All-Union Conf. "Liquid Crystals and Their Practical Applications" (Ivanovo, 1985) Vol. 1, Book 2 (Ivanovo: Izd. Ivan. Gos. Univ., 1985) p. 199
51. Hauser A et al. *Cryst. Res. Technol.* **19** 261 (1984)
52. Umstätter H, in *Einführung in die Viskosimetrie und Rheometrie* (Ed. H Umstätter) (Berlin: Springer, 1952) c. 91
53. Meiboom S, Hewitt R C *Phys. Rev. Lett.* **30** 261 (1973)
54. Derfel G *Mol. Cryst. Liq. Cryst.* **191** 377 (1990)
55. Khazimullin M V et al. *Mol. Cryst. Liq. Cryst.* **329** 247 (1999)
56. Yablonsky S V et al. *Proc. SPIE* **2731** 87 (1996)
57. Oliveira E A, Figueiredo Neto A M, Durand G *Phys. Rev. A* **44** R825 (1991)
58. Vorflusev V P, Kitzerow H, Chigrinov V G *Appl. Phys.* **55** 1145 (1996)
59. Krekhov A P, Chuvyrov A N *Mol. Cryst. Liq. Cryst.* **192** 251 (1990)
60. Krekhov A P, Reiter A V, Sevost'yanov V P, in *Tez. Dokl. 6 Vses. Konf. "Zhidkie Kristally i Ikh Prakticheskoe Ispol'zovanie"* (*Chernigov, 1988*) T. 6 (Abstr. 6 All-Union Conf. "Liquid Crystals and Their Practical Applications" (Chernigov, 1988) Vol. 6 (Chernigov: Izd. Chernigov. Gos. Ped. Inst., 1988) p. 470
61. Wahl J, Fischer F *Mol. Cryst. Liq. Cryst.* **22** 359 (1973)
62. Waltermann Th, Fischer F *Z. Naturforsch.* **30a** 519 (1975)
63. Fischer F, Wahl J, Waltermann Th *Ber. Bunsenges.* **78** 891 (1974)
64. Holmstroem S, Lagerwall S T *Mol. Cryst. Liq. Cryst.* **38** 141 (1977)
65. Yablonskiĭ S V et al. *Kristallografiya* **29** 984 (1984)
66. Grupp J *Rev. Sci. Instrum.* **54** 754 (1983)
67. Kuss E *Mol. Cryst. Liq. Cryst.* **47** 71 (1978)
68. Diogo A C *Solid State Commun.* **50** 895 (1984)
69. Martinoty P, Candau S *Mol. Cryst. Liq. Cryst.* **14** 243 (1971)
70. Tabidze A A, Koshkin N I, Dep. VINITI No 2081-B88 (Deposited Inst. Sci. Tech. Inform. No 2081-V88) (Moscow, 1988) p 1
71. Tabidze A A, Koshkin N I, Novosyolov V I *Izmerit. Tekhn.* (12) 59 (1981)
72. D'yachenko B P Diss...kand. fiz.-mat. nauk (Theses Sci. Degree. Cand. Fiz. Math. Sci.) (Kuibyshev, 1973)
73. Tabidze A A, Kazakov R Kh *Izmerit. Tekhn.* (1) 34 (1983)
74. Tabidze A A, Koshkin N I *Zh. Fiz. Khim.* **60** 1501 (1986)
75. Langevin D, Bouchiat M A *J. Phys.* (Paris) **33** 101 (1972)
76. Langevin D, Bouchiat M A *Mol. Cryst. Liq. Cryst.* **22** 317 (1973)
77. McQueen D H, Singhal V K *J. Phys. D: Appl. Phys.* **7** 1983 (1974)
78. Tsvetkov V N *Zh. Eksp. Teor. Fiz.* **9** 602 (1939)
79. Tsvetkoff V N *Acta Physicochim. URSS* **10** 555 (1939)
80. Prost J, Gasparoux H *Phys. Lett. A* **36** 245 (1971)
81. Gasparoux H, Prost J *J. Phys.* (Paris) **32** 65 (1971)
82. Siedler L T S et al. *Mol. Cryst. Liq. Cryst.* **90** 255 (1983)
83. Leslie F M, Luckhurst G R, Smith H J *Chem. Phys. Lett.* **13** 368 (1972)
84. Kneppe H, Schneider F *J. Phys. E: Sci. Instrum.* **16** 512 (1983)
85. Yun C K *Phys. Lett. A* **45** 119 (1973)
86. Lippmann H *Ann. Phys.* (Leipzig) **1** 157 (1958)
87. de Gennes P G *The Physics of Liquid Crystals* (Oxford: Clarendon Press, 1974) [Translated into Russian (Moscow: Mir, 1977)]
88. Brochard F *Mol. Cryst. Liq. Cryst.* **23** 51 (1973)
89. Helfrich W *Phys. Rev. Lett.* **21** 1518 (1968)
90. Anisimov M M, Lagunov A S *Zh. Fiz. Khim.* **56** 1316 (1982)
91. Bogdanov D L, Lagunov A S, Luk'yanov A E, Avt. Svid. (USSR Inventor's Certificate) No 731355; Bull. Izobr. (16) (1980)
92. Bogdanov D L, Gevorkyan E V, Lagunov A S *Akust. Zh.* **26** 28 (1980)
93. Lagunov A S, Larionov A N *Akust. Zh.* **30** 344 (1984)
94. Doerrer H et al. *Liq. Cryst.* **1** 573 (1986)
95. Gevorkyan E V, Lagunov A S, Ergashev D *Akust. Zh.* **28** 14 (1982)
96. Lagunov A S, Larionov A N *Akust. Zh.* **30** 344 (1984)
97. Lagunov A S, Larionov A N, Ergashev D, in *10 Vses. Akustich. Konf.* (*Moscow, 1983*) (10th All-Union Acoustic Conference) (Moscow: Izd. Akust. Inst. AN SSSR) p. 56
98. Lagunov A S, Gevorkyan E V, Larionov A N, in *Zhidkie Kristally,* Mezhvuz. Sb. Nauch. Trudov (Liquid Crystals, Proceed. Sci. Conf) (Ivanovo: Izd. Ivan. Gos. Univ., 1985) p. 23
99. Lagunov A S, in *Abstracts of 10th Int. Liq. Cryst. Conf.* (New York, 1984) p. 23
100. Kozhevnikov E N *Akust. Zh.* **40** 412 (1994) [*Acoust. Phys.* **40** 369 (1994)]
101. Bogdanov D L, Lagunov A S, Larionov A N *Zh. Fiz. Khim.* **71** 931 (1997)
102. Bogdanov D L, Larionov A N, Pasechnik S V, in *Abstracts of 17th Int. Liq. Cryst. Conf.* (Strasbourg, France, 1998)
103. Bogdanov D L, Vekovishchev M P, in *Tez. Dokl. Vseross. Nauch.-Tekh. Konf.* (Abstr. All-Russia sci.-tech. conf.) (Voronezh, 1997)
104. Lagunov A S, Anikin A M *Zh. Fiz. Khim.* **60** 417 (1986)

105. Bogdanov D L, Diss...dokt. fiz.-mat. nauk (Theses Sci. Degree Doct. Fiz. Math. Sci.) (Moscow, 1999)
106. Gerber P R *Appl. Phys. A* **26** 139 (1981)
107. Schad Hp, Baur G, Meier G *Appl. Phys.* **17** 177 (1978)
108. Rep'eva A, Frederiks V, in *V S'ezd Russkikh. Fizikov* (5th Congr. Russian Physicists) (Moscow: GIZ, 1926)
109. Chigrinov V G *Kristallografiya* **27** 404 (1982)
110. Stephen M J, Straley J P *Rev. Mod. Phys.* **46** 617 (1974)
111. Van Dijk J W, Beens W W, de Jeu W H *J. Chem. Phys.* **79** 3888 (1983)
112. Cladis P *Phys. Rev. Lett.* **28** 1628 (1972)
113. Leenhouts F, Dekker A J *J. Chem. Phys.* **74** 1956 (1981)
114. Chigrinov V G, Grebenkin M F *Kristallografiya* **20** 1241 (1975)
115. Schad Hp *J. Appl. Phys.* **54** 4994 (1983)
116. Pasechnik S V et al. *J. Phys.* (Paris) **45** 441 (1984)
117. Pasechnik S V, Diss...dokt. fiz.-mat. nauk (Theses Sci. Degree Doct. Fiz. Math. Sci.) (Moscow, 1998)
118. Leenhouts F *J. Appl. Phys.* **58** 2180 (1985)
119. Belyaev V V et al., in *Tez. Dokl. 3 Nauch.-Tekh. Seminara "Opticheskie Svoĭstva Zhidkikh Kristallov i Ikh Primenenie"* (*Leningrad, 1983*) (Optical Properties of Liquid Crystals and Their Application: Abstr. 3d Sci.-Tech. Workshop) (Leningrad: Gos. Opt. Inst. Im. S I Vavilova, 1983) p. 51
120. Petrov V F et al., in *Tez. Dokl. 3 Nauch.-Tekh. Seminara "Opticheskie Svoĭstva Zhidkikh Kristallov i Ikh Primenenie"* (*Leningrad, 1983*) (Optical Properties of Liquid Crystals and Their Application: Abstr. 3d Sci.-Tech. Workshop) (Leningrad: Gos. Opt. Inst. Im. S I Vavilova, 1983) p. 49
121. Kuhn W L, Finlayson B A *Mol. Cryst. Liq. Cryst.* **36** 307 (1976)
122. Imai M et al. *Mol. Cryst. Liq. Cryst.* **262** 267 (1995)
123. Hess S, Pardowitz I *Z. Naturforsch.* **36a** 1224 (1981)
124. Hess S *Z. Naturforsch.* **30a** 554 (1975)
125. Derfel G, Gajewska B *Proc. SPIE* **3318** 292 (1998)
126. Sadovskiĭ V N, Usova N A, in *Tez. Dokl. 6 Vses. Konf. "Zhidkie Kristally i Ikh Prakticheskoe Ispol'zovanie"* (*Chernigov, 1988*) T. 3 (Abstr. 6 All-Union Conf. "Liquid Crystals and Their Practical Applications" (Chernigov, 1988) Vol. 2 (Chernigov: Izd. Chernigov. Gos. Ped. Inst., 1988) p. 194; Sadovskiĭ V N, Usova N A *Kristallografiya* **35** 1504 (1990) [*Sov. Phys. Cryst.* **35** 886 (1990)]
127. Sadovskiĭ V N, Usova N A *Akust. Zh.* **33** 551 (1987)
128. Tabiryan N V, Sukhov A V, Zel'dovich B Ya *Mol. Cryst. Liq. Cryst.* **136** 1 (1986)
129. Umeton C, Cipparrone G, Duca D *Mol. Cryst. Liq. Cryst.* **261** 187 (1995)
130. Leger L *Solid State Commun.* **10** 697 (1972)
131. Wang X *Phys. Lett. A* **112** 402 (1985)
132. Geurst J A, Spruijt A M, Gerritsma C J *J. Phys.* (Paris) **36** 653 (1975)
133. Allen S M, Cahn J W *Acta Metall.* **27** 1085 (1979)
134. Orihara H, Ishibashi Y *J. Phys. Soc. Jpn.* **55** 2151 (1986)
135. Ohta T, Jasnow D, Kawasaki K *Phys. Rev. Lett.* **49** 1223 (1982)
136. Grigutsch M et al. *Mol. Cryst. Liq. Cryst.* **261** 283 (1995)
137. Lonberg F et al. *Phys. Rev. Lett.* **52** 1903 (1984)
138. Orsay Liquid Crystals Group *J. Chem. Phys.* **51** 816 (1969)
139. Orsay Liquid Crystals Group *Phys. Rev. Lett.* **22** 1361 (1969)
140. Leger-Quercy L "Etude experimentale des fluctuations thermiques d'orientation dans un crystal liquide nematique par diffusion inelastique de la lumiere" Thesis (Paris: University of Paris, 1970)
141. Van Eck D C, Perdeck M *Mol. Cryst. Liq. Cryst.* **49** 39 (1978)
142. Van Eck D C, Westera W *Mol. Cryst. Liq. Cryst.* **38** 319 (1977)
143. Ivanov S A, Vetrov V Yu, Dep. VINITI No 4978-80 (Deposited Inst. Sci. Tech. Inform. No 4978-80) (Moscow, 1980) p 1
144. Ivanov S A, Vetrov V Yu *Kristallografiya* **27** 11014 (1982)
145. Ivanov S A, Vetrov V Yu *Zh. Prikl. Spektrosk.* **37** 316 (1982)
146. Van der Meulen J P, Zijlstra R J J *J. Phys.* (Paris) **45** 1627 (1984)
147. Cummins H Z, Pike E R (Eds) *Photon Correlation and Light Beating Spectroscopy* (New York: Plenum Press, 1974) [Translated into Russian (Moscow: Mir, 1978)]
148. Leslie F M, Waters C M *Mol. Cryst. Liq. Cryst.* **123** 101 (1985)
149. Hirakata J et al. *Jpn. J. Appl. Phys. Pt. 2* **25** L607 (1986)
150. Akiyama R et al. *Jpn. J. Appl. Phys. Pt. 2* **25** L769 (1986)
151. Miraldi E et al. *Nuovo Cimento* **60** 165 (1980)
152. Hanmer J M W, Coles H J *Mol. Cryst. Liq. Cryst.* **262** 235 (1995)
153. Belyaev V V, Ivanov S A, Grebenkin M F *Kristallografiya* **30** 1160 (1985)
154. Belyaev V V, in *Physical Properties of Liquid Crystals: Nematics* (Eds D A Dunmur, A Fukuda, G R Luckhurst) (London: IEE, 2000) p. 414
155. Moscicki J K , in *Physical Properties of Liquid Crystals: Nematics* (Eds D A Dunmur, A Fukuda, G R Luckhurst) (London: IEE, 2000) p. 387
156. Martins A F, in *Physical Properties of Liquid Crystals: Nematics* (Eds D A Dunmur, A Fukuda, G R Luckhurst) (London: IEE, 2000) p. 405
157. Belyaev V V *Usp. Khim.* **60** 1601 (1989)
158. Belyaev V V *Izv. Ross. Akad. Nauk Ser. Fiz.* **60** (4) 12 (1996) [*Bull. Russ. Acad. Sci.* **60** 512 (1996)]